Institute for Scientific Information® CITATION DATABASES

HOME HELP GENERAL SEARCH CITED REF SEARCH MARK LOG OFF

General Search Results--Full Record

Article 11 of 28 PREVIOUS NEXT SUMMARY RELATED RECORDS

Convective **transport of biomass burning emissions over Brazil during TRACE A**
Pickering KE, Thompson AM, Wang YS, Tao WK, McNamara DP, Kirchhoff VWJH, Heikes BG, Sachse GW, Bradshaw JD, Gregory GL, Blake DR
JOURNAL OF GEOPHYSICAL RESEARCH-ATMOSPHERES
101: (D19) 23993-24012 OCT 30 1996

Document type: Article **Language:** English **Cited References:** 17 **Times Cited:** 50

Abstract:
A series of large mesoscale **convective** systems that occurred during the Brazilian phase of GTE/TRACE A (Transport and Atmospheric Chemistry near the Equator-Atlantic) provided an opportunity to observe deep **convective** transport of trace gases from biomass burning. This paper reports a detailed analysis uf flight 6, on September 27, 1992, which sampled cloud- and biomass-burning-perturbed regions north of Brasilia. High-frequency sampling of cloud outflow at 9-12 km from the NASA DC-8 showed enhancement of CO mixing ratios typically a factor of 3 above background (200-300 parts per billion by volume (ppbv) versus 90 ppbv) and significant increases in NO, and hydrocarbons, Clear signals of lightning-generated NO were detected; we estimate that at least 40% of NOx at the 9.5-km level and 32% at 11.3 km originated from lightning, Four types of model studies have been performed to analyze the dynamical and photochemical characteristics of the series of **convective** events. (1) Regional simulations for the period have been performed with the NCAR/Penn State mesoscale model (MM5), including tracer transport of carbon monoxide, initialized with observations. Middle-upper tropospheric enhancements of a factor of 3 above background are reproduced. (2) A cloud-resolving model (the Goddard cumulus ensemble (GCE) model) has been run for one representative **convective** cell during the September 26-27 episode. (3) Photochemical calculations (the Goddard tropospheric chemical model), initialized with trace gas observations (e.g., CO, NOx, hydrocarbons, O-3) observed in cloud outflow, show appreciable O-3 formation postconvection, initially up to 7-8 ppbv O-3/d. (4) Forward trajectories from cloud outflow levels (postconvective conditions) put the ozone-producing air masses in eastern Brazil and the tropical Atlantic within 2-4 days and over the Atlantic, Africa, and the Indian Ocean in 6-8 days, Indeed, 3-4 days after the **convective** episode (September 30, 1992), upper tropospheric levels in the Natal ozone sounding show an average increase of similar to 30 ppbv (3 Dobson units (DU) integrated) compared to the September 28 sounding. Our simulated net O-3 production rates in cloud outflow are a factor of 3 or more greater than those in air undisturbed by the storms, Integrated over the 8- to 16-km cloud outflow layer, the postconvection net O-3 production (similar to 5-6 DU over 8 days) accounts for similar to 25% of the excess O-3 (15-25 DU) over the South Atlantic. Comparison of TRACE A Brazilian ozonesondes and the frequency of deep convection with climatology [Kirchhoff et al., this issue] suggests that the late September 1992 conditions represented an unusually active period for both convection and upper tropospheric ozone formation.

KeyWords Plus:
TROPOSPHERIC OZONE, AIR

Addresses:
Pickering KE, UNIV MARYLAND, JOINT CTR EARTH SYST SCI, DEPT METEOROL, CODE 916, COLLEGE PK, MD 20742.
NASA, GODDARD SPACE FLIGHT CTR, GREENBELT, MD 20771.
SCI SYST & APPLICAT INC, LANHAM, MD 20706.
UNIV CALIF IRVINE, IRVINE, CA 92717.
GEORGIA INST TECHNOL, ATLANTA, GA 30332.
NASA, LANGLEY RES CTR, HAMPTON, VA 23681.
UNIV RHODE ISL, GRAD SCH OCEANOG, NARRAGANSETT, RI 02882.
APPL RES CORP, LANDOVER, MD 20785.
INST NACL PESQUISAS ESPACIAIS, S JOSE CAMPOS, BRAZIL.

Publisher:
AMER GEOPHYSICAL UNION, WASHINGTON

IDS Number:
VQ493

ISSN:
0148-0227

Article 11 of 28 PREVIOUS NEXT SUMMARY

Copyright © 2002 Institute for Scientific Information

JOURNAL OF GEOPHYSICAL RESEARCH, VOL. 101, NO. D19, PAGES 23,993–24,012, OCTOBER 30, 1996

Convective transport of biomass burning emissions over Brazil during TRACE A

Kenneth E. Pickering,[1] Anne M. Thompson,[1,2] Yansen Wang,[3] Wei-Kuo Tao,[2]
Donna P. McNamara,[4] Volker W. J. H. Kirchhoff,[5] Brian G. Heikes,[6]
Glen W. Sachse,[7] John D. Bradshaw,[8] Gerald L. Gregory,[7] and Donald R. Blake[9]

Abstract. A series of large mesoscale convective systems that occurred during the Brazilian phase of GTE/TRACE A (Transport and Atmospheric Chemistry near the Equator–Atlantic) provided an opportunity to observe deep convective transport of trace gases from biomass burning. This paper reports a detailed analysis of flight 6, on September 27, 1992, which sampled cloud- and biomass-burning-perturbed regions north of Brasilia. High-frequency sampling of cloud outflow at 9–12 km from the NASA DC-8 showed enhancement of CO mixing ratios typically a factor of 3 above background (200–300 parts per billion by volume (ppbv) versus 90 ppbv) and significant increases in NO_x and hydrocarbons. Clear signals of lightning-generated NO were detected; we estimate that at least 40% of NO_x at the 9.5-km level and 32% at 11.3 km originated from lightning. Four types of model studies have been performed to analyze the dynamical and photochemical characteristics of the series of convective events. (1) Regional simulations for the period have been performed with the NCAR/Penn State mesoscale model (MM5), including tracer transport of carbon monoxide, initialized with observations. Middle-upper tropospheric enhancements of a factor of 3 above background are reproduced. (2) A cloud-resolving model (the Goddard cumulus ensemble (GCE) model) has been run for one representative convective cell during the September 26–27 episode. (3) Photochemical calculations (the Goddard tropospheric chemical model), initialized with trace gas observations (e.g., CO, NO_x, hydrocarbons, O_3) observed in cloud outflow, show appreciable O_3 formation postconvection, initially up to 7–8 ppbv O_3/d. (4) Forward trajectories from cloud outflow levels (postconvective conditions) put the ozone-producing air masses in eastern Brazil and the tropical Atlantic within 2–4 days and over the Atlantic, Africa, and the Indian Ocean in 6–8 days. Indeed, 3–4 days after the convective episode (September 30, 1992), upper tropospheric levels in the Natal ozone sounding show an average increase of ~30 ppbv (3 Dobson units (DU) integrated) compared to the September 28 sounding. Our simulated net O_3 production rates in cloud outflow are a factor of 3 or more greater than those in air undisturbed by the storms. Integrated over the 8- to 16-km cloud outflow layer, the postconvection net O_3 production (~5–6 DU over 8 days) accounts for ~25% of the excess O_3 (15–25 DU) over the South Atlantic. Comparison of TRACE A Brazilian ozonesondes and the frequency of deep convection with climatology [*Kirchhoff et al.*, this issue] suggests that the late September 1992 conditions represented an unusually active period for both convection and upper tropospheric ozone formation.

[1]Joint Center for Earth System Science, University of Maryland, College Park.
[2]NASA Goddard Space Flight Center, Greenbelt, Maryland.
[3]Science, Systems, and Applications, Inc, Lanham, Maryland.
[4]Applied Research Corporation, Landover, Maryland.
[5]INPE, Sao Jose dos Campos, SP, Brazil.
[6]Graduate School of Oceanography, University of Rhode Island, Narragansett.
[7]NASA/Langley Research Center, Hampton, Virginia.
[8]Georgia Institute of Technology, Atlanta.
[9]University of California-Irvine, Irvine.

Copyright 1996 by the American Geophysical Union.

Paper number 96JD00346.
0148-0227/96/96JD-00346$09.00

1. Introduction

Deep convection is a major component of the atmospheric general circulation. Regions of convection that form important upward branches of the Walker circulation are located on the eastern and western edges of the study region for the NASA GTE/TRACE A experiment. This paper focuses on deep convection that occurred over the western part of the study region, the interior of Brazil, during the field mission.

Chatfield and Crutzen [1984] hypothesized that deep convection is a major redistributor of trace gases from the boundary layer to the free troposphere, and *Dickerson et al.* [1987] presented observational evidence that such redistribution occurs. *Pickering et al.* [1990] showed that once ozone precursor gases are transported to the middle and upper troposphere by deep convection, ozone production in the cloud outflow can be substantially enhanced. *Pickering et al.* [1991] used measurements from a previous NASA/GTE field mission in Brazil (Amazon Boundary Layer Expedition (ABLE) 2A) in studying the effects on ozone production of a dry season squall line over Amazonia, using a convective cloud model and a photochemical model in tandem. A pollution plume from distant biomass fires was evident in these measurements. When convectively lifted, this pollution was capable of converting a significant layer from one of O_3 destruction to one of O_3 production. In the *Pickering et al.* [1992a] paper we performed a sensitivity study using the cloud dynamics of the ABLE 2A event to examine the effects of deep convection on ozone production in two scenarios with relatively fresh biomass burning pollution. With an assumption of a pristine upper troposphere we found that column ozone production in cloud outflow may be enhanced by at least a factor of 50. *Chatfield and Delany* [1990] used a "traveling one-dimensional" model to also estimate the downstream effects of convective transport of biomass burning pollution. *Kirchhoff and Marinho* [1994] have noted evidence of convective transport of ozone in ozonesonde profiles taken over Brazil during the burning season. *Chatfield and Delany* [1990] and *Pickering et al.* [1992a] hypothesized that ozone produced in this manner could be transported over the South Atlantic and could contribute to the ozone maximum detected by satellite [*Fishman et al.*, 1990; *Watson et al.*, 1990]. While contributing a relatively smaller amount to total column O_3 than similar concentrations in the lower troposphere, the O_3 produced in the upper troposphere as a result of convective transport has greater importance for climate forcing [*Lacis et al.*, 1990].

The aircraft missions during the TRACE A experiment were aimed at sampling all of the major features of the circulation contributing air to the region of the South Atlantic ozone maximum. During the Brazilian component of the experiment a major series of deep convective systems developed over the cerrado. One of the flights (flight 6) from the TRACE A base in Brasilia was devoted to sampling the outflow from these systems, although some cloud-processed air was also noted on flight 5 (along the Brazilian coast) and flight 7 (over the cerrado). These flights document the large-scale effects of deep convection on trace gas distributions in the South Atlantic region. Ozonesonde measurements show the impact of upper level transport of ozone from the cerrado region of Brazil to Natal and to a number of more distant locations [See *Thompson et al.*, this issue]. The combination of aircraft and ozonesonde measurements provides the opportunity to verify our previous model results concerning transport of biomass burning emissions and subsequent downstream ozone production.

We document the occurrence of a major series of deep convective episodes during the latter part of the cerrado burning season in 1992. We present trace gas measurements taken from the NASA DC-8 and a Brazilian aircraft that are representative of the low-altitude pollution related to biomass burning and of the outflow from the deep convection that occurred on September 26–27, 1992. Because the aircraft measurements in cloud-processed air were of limited spatial and temporal duration, we use a sequence of mesoscale and cloud-resolving model simulations to extend the measurements to determine the full extent of the effects of the convective systems on regional trace gas distributions. A detailed description of the mesoscale (MM5) modeling activity for the September 26–27 events is given by *Wang et al.* [this issue]. We also use the three-dimensional Goddard cumulus ensemble (GCE) model to simulate one representative convective cell, providing wind fields for use in transport calculations for a variety of species. Forward trajectories are computed using the methods recommended by *Pickering et al.* [this issue] to determine the long-range transport of the cloud outflow at upper levels. A photochemical box model (similar to the GSFC one-dimensional tropospheric model used in our previous studies) is used to estimate the net ozone production during the downstream transport. This ozone production proceeds at the rate of several parts per billion by volume (pppv) per day, as these air masses are transported in upper level westerlies over the South Atlantic.

Section 2 of this paper presents a description of the convective events leading up to flight 6, as well as their relationship to the biomass fires in the cerrado region. In section 3 we display and discuss the trace gas measurements made on flight 6 and on a flight of the Brazilian aircraft. Section 4 describes the use of measurements from undisturbed air to provide initial conditions for our mesoscale model simulation of the major convective systems immediately preceding flight 6. Tracer transport results for CO are also presented in this section and compared with DC-8 observations in cloud-processed air. Section 5 presents a simulation with the GCE model of one convective cell contained within one of the systems sampled on flight 6. We also present cloud-scale tracer transport results for other species such as NO_x, O_3, and total nonmethane hydrocarbon (NMHC). In section 6 we show 8-day forward trajectories from the cloud systems and from the measurement locations, as well as photochemical calculations of ozone production along these transport paths. Our ozone production estimates summed over the first four days of transport compare favorably with the upper tropospheric ozone increase at Natal, Brazil, noted in ozonesonde measurements following the convective episode. In section 7 we conclude with a summary of the impact of the Brazilian convection on ozone in the South Atlantic region.

2. Synoptic Conditions

2.1. Meteorology

The 1992 dry season over much of the cerrado region of Brazil ended earlier than normal with a number of cold fronts arriving from the southwest producing shower activity during September. Rainfall statistics for the region are given by *Kirchhoff et al.* [this issue]. An abnormally high frequency of deep convection is also noted from satellite measurements of out-

going longwave radiation (see Figures 1a–1d). In September, almost all of Brazil is seen to have monthly mean values of outgoing longwave radiation less than the 1979–1988 average. Values lower than normal indicate a greater amount of deep convection than normal. The September anomaly exceeded 30 W m^{-2} over a large region to the west of Brasilia. In October the pattern continued with abnormally low values of outgoing longwave radiation (abnormally high frequency of deep convection) over all of Brazil between 10°S and 25°S, but the anomaly was not so extreme as in September.

During the TRACE A DC-8 flights in Brazil a major outbreak of deep convection developed over the region (September 22–28). The series of convective events began in southern

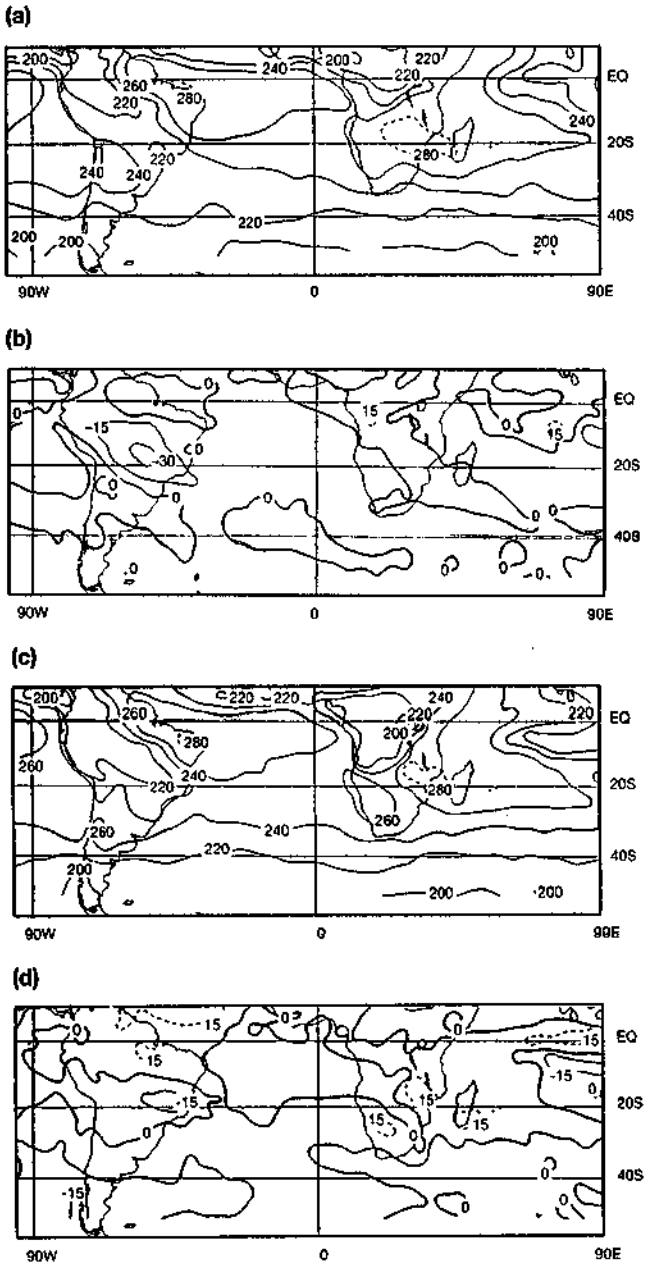

Figure 1. Outgoing longwave radiation (W m^{-2}) from NOAA 11 AVHRR IR window channel. (a) September 1992 mean; (b) September 1992 anomaly; (c) October 1992 mean; (d) October 1992 anomaly. Anomalies are departures from 1979 to 1988 means for each month.

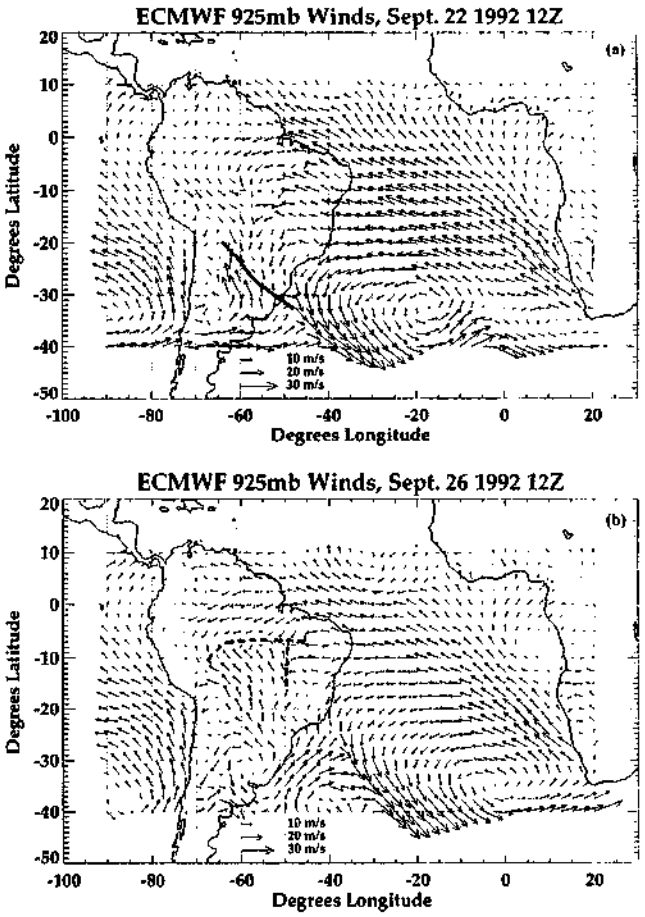

Figure 2. ECMWF wind vector plots at 925 mbar for 1200 UT on (a) September 22, (b) September 26, 1992. Frontal position (solid line) shown for September 22 and lines of convergence (dashed lines) shown for September 26.

Brazil associated with a cold frontal system pushing northeastward from the midlatitudes of the southern hemisphere. The frontal position on September 22 is depicted on the 925-mbar wind vector plot in Figure 2a. Thundershower activity on September 22 was noted as far north as Cuiaba (~16°S, 57°W). The front remained nearly stationary on September 23 and 24 with convective activity to the north of the front, although at the surface little thermal contrast remained across the front. However, a strong zone of low-level convergence persisted over the region continuing to induce deep convective activity. The front rapidly advanced to the north between 1200 UT September 25 and 1200 UT September 26 [see *Bachmeier and Fuelberg*, this issue]. Storms occurred as far north and east as 8°S and 50°W on September 25. Large mesoscale convective systems developed on September 26 even farther to the north and east (see Meteosat 4 imagery in Plate 1) and continued through the early morning hours of September 27. These systems are associated with the zones of convergence seen in Figure 2b.

The more northerly line of convection (centered on about 8°S) developed first (before 1530 UT on September 26). A line of storms extended from approximately 46° to 60°W. The storms in this line reached maximum intensity at about 1830 UT (Plate 1a), with some cloud top temperatures below 195 K, indicating cloud top altitudes of at least 16 km. A more southerly (10°–15°S) north-south oriented line located between 45°

and 50° W developed by 2130 UT and reached maximum intensity between 2130 UT on September 26 and 0330 UT (Plate 1b) on September 27. Digital imagery is not available in this time interval, but low-resolution Meteosat 3 imagery received in the field suggests peak development about 0130 UT on September 27. Cloud top temperatures in this system were less than 205 K at 2130 UT, equivalent to cloud top heights of at least 15 km. These systems occurred over regions of biomass burning activity, and TRACE A flight 6 was designed to capture the outflow from these storms. The approximate flight track for flight 6 (flown from ~0900 to ~1630 UT on September 27) is superimposed on the satellite imagery. It is these systems on September 26 and 27 that we simulate with MM5. One cell from the second system is simulated with the Goddard cumulus ensemble model.

2.2. Biomass Fires

A weekly record of fire pixel counts estimated from the AVHRR instrument onboard the NOAA satellites has been provided by A. Setzer of INPE. Figure 3 shows the weekly averaged fire pixel counts per day from mid-August through the end of October 1992, for the region in which the DC-8 flights (flights 6 and 7) over Brazilian biomass burning were conducted. Peak fire counts per day (approximately 2000) were detected during the August 28 to September 3 period. By the time the DC-8 reached Brasilia (week of September 25 to October 1), the daily average had declined to approximately 700 per day, or about one third of the peak weekly value in the period shown.

The AVHRR data were processed at NASA Goddard Space Flight Center for the individual days during the September 25 to October 1 period, using the algorithm of *Justice et al.* [this issue] (SAFARI JGR special issue). This is the same algorithm used for fire counts in Africa during the SAFARI and TRACE A experiments. We use the Justice fire count product (available in the form of daily fire counts for 0.5° latitude by 0.5° longitude grid cells) for the two days (September 25 and 26 at ~1830 LT) preceding flight 6 in constructing initial conditions for a regional CO transport simulation (see section 4). Regions of cloudiness prevented fire count observations over large areas of interest on September 26. However, major areas of fires were noted to the north and northeast of Brasilia. The second (more southerly) major convective system described in section 2.1 developed over the major region of biomass fires that were detected on September 26 north of Brasilia. The earlier system was fed with polluted air by low-level easterly winds from fires farther to the east. The most concentrated burning activity on these days was located in the state of Amazonas, well to the northwest of the flight region.

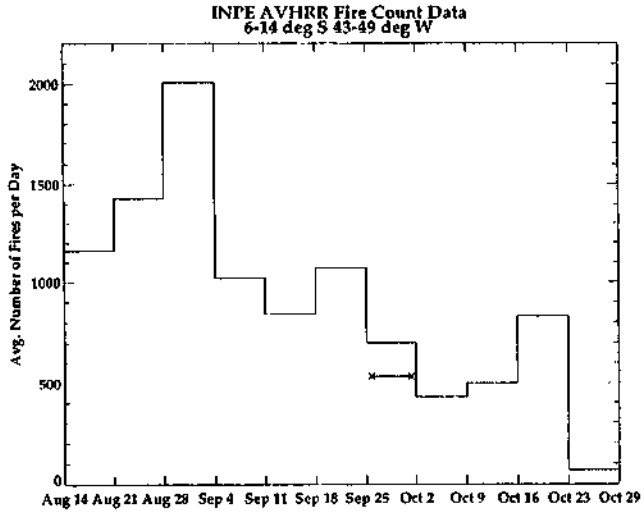

Figure 3. INPE AVHRR fire pixel counts: average number of fire pixels per day by week from mid-August to October 1992, for TRACE A flight region in Brazil. Daily average fire pixel count for September 25 to October 1 estimated with algorithm of *Justice et al.* [this issue] is shown with horizontal line. Justice et al. value is approximately 25% lower than the INPE value. The difference is likely due to fewer instances of hot surfaces from daytime solar heating being detected with the Justice algorithm.

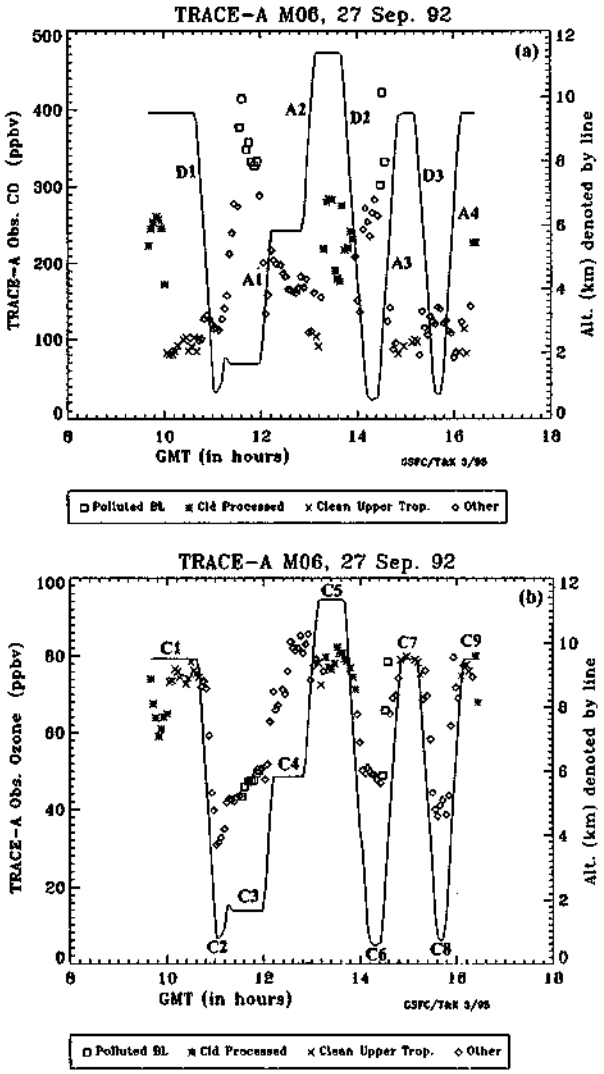

Figure 4. Summary of DC-8 chemical measurements on TRACE A flight 6 (a) O_3, (b) CO. Ascents (A), descents (D), and constant-altitude (C) legs are indicated. Three regimes are denoted with indicated symbols and defined as follows: polluted BL, altitude <4 km and CO >300 ppbv; cloud-processed, altitude >6 km and CO >150 ppbv, and clean upper troposphere, altitude >6 km and CO <120 ppbv.

3. Chemical Measurements

The DC-8 flights designed to characterize Brazilian biomass burning emissions and outflow from the continent began with

a flight (flight 5) from Natal, Brazil, southward along the east coast of Brazil to a point south of Rio de Janeiro and then inland to Brasilia. This flight characterized the continental inflow at low levels and outflow at upper levels. There were two local flights from Brasilia: flight 6 to examine convective outflow and flight 7 to characterize the emissions from fires in the Brazilian cerrado. The following subsections describe the flight 6 and related INPE aircraft measurements from September 27 in depth. Section 3.1 describes measurements from both aircraft in air undisturbed by the convection, while section 3.2 contains a discussion of the DC-8 measurements in cloud-processed air.

Observations of O_3 and CO (3-minute averages) during flight 6 are summarized in Figure 4, along with a depiction of the various ascents, descents, and constant-altitude segments. A number of altitudes were flown in an attempt to capture outflow from the convective systems described in section 2. Because CO is a good tracer of convective transport from the boundary layer, we define cloud outflow regions using a combination of measured CO mixing ratios and satellite imagery. Enhanced upper tropospheric (>6 km) CO mixing ratios measured in areas within or downwind of cold cloud tops seen on IR satellite imagery were considered to be indicative of cloud outflow. See Table 5 for exact definitions of this and other regimes. Cloud-processed CO appears as a mixture of clean upper tropospheric air and air convectively lifted from lower-altitude polluted layers. Outflow was encountered on the first 9.5-km flight leg, at the 11.3-km level, on the ascent to and the descent from the 11.3-km leg, and again on the final 9.5-km flight leg. On the remainder of the flight the air appeared to be undisturbed by the cloud systems. For O_3 the cloud-processed air is evident from the mixing ratios that are lower than others at that altitude (i.e., lower O_3 air has been convectively mixed upward to that altitude).

3.1. Observations in Undisturbed Air

We have thoroughly analyzed the trace gas observations in undisturbed air for the purpose of deriving initial conditions for transport modeling. In this subsection we describe only the CO observations, as indicative of the pollution found in this region. Figure 5 shows detailed CO profiles (5-s data) for two of the several ascents and descents depicted in Figure 4) that were in primarily undisturbed air. Air polluted from biomass burning on descent 2 is easily distinguished from relatively clean air on descent 1. Pollution in the air undisturbed by the cloud systems is typically evident at altitudes less than 5 km. In addition to the lower portion of descent 2, very polluted layers are evident on ascents 1 and 3, with CO exceeding 300 ppbv on each of these profiles. One plume between 3 and 3.5 km on ascent 3 contained >1 ppmv CO. Most of these polluted layers likely resulted from fires on the previous day (September 26) because little burning on the September 27 was evident until the latter portion of the flight. In contrast, the clean air profiles (ascent 4, descents 1 and 3) have CO mixing ratios typically between 100 and 130 ppb in the lower levels. The contrast between clean and polluted air is also evident on the constant-altitude segments in regions undisturbed by the cloud systems (Figure 6). For example, constant-altitude segments 3 and 6 show mean CO values of 320 ppbv (36-min average) and 270 ppbv (6-min average). On the other hand, relatively clean continental air ([CO] = 140–150 ppbv) was found on constant-altitude segments 2 and 8. In the upper troposphere, most of the profiles and the constant-altitude segments show CO to be in the range 80–100 ppbv in undisturbed air.

The INPE aircraft flew primarily in moderately polluted air and purposely avoided relatively fresh heavily polluted plumes. The aircraft typically took measurements intensively in a smaller region than the DC-8, sampling at seven designated altitudes, from below 1 km to just over 3.5 km. The flight on September 27 was flown from Porto Nacional to the vicinity of 10°S 54°W, and the profile sampling began at 1220 UT (0920 LT). Moderate pollution was found at the three levels below 2 km with CO mixing ratios in the 200–235 ppbv range (Figure 7). This flight also occurred before the typical time of day that biomass fires begin [*Prins and Menzel*, 1994]. These values are therefore representative of moderate biomass burning pollution that had aged a day or more. Above 2 km the CO mixing ratios decline to the 120–145 ppbv range.

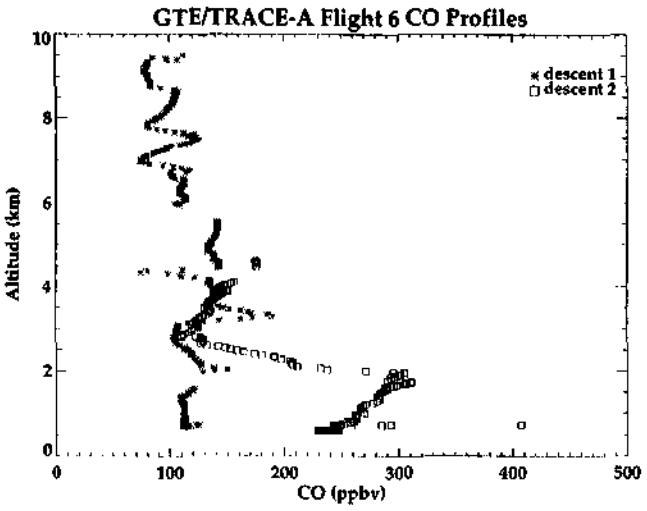

Figure 5. Profiles of CO from flight 6 (5-s CO data) in air undisturbed by convection on descents 1 (clean) and 2 (polluted).

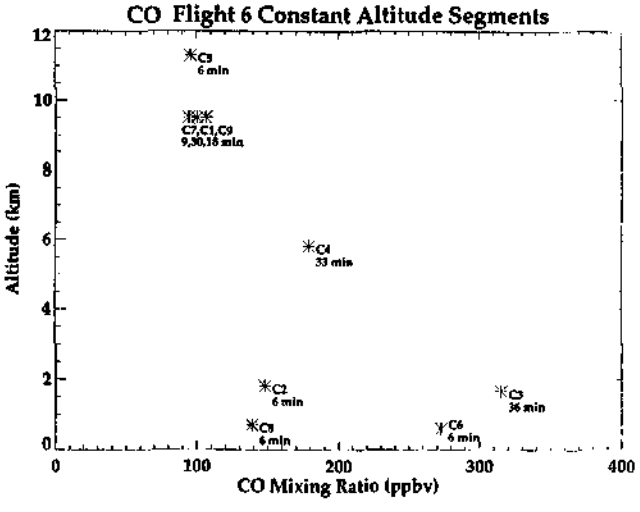

Figure 6. Average CO (ppbv) on indicated constant-altitude flight legs for flight 6 in air undisturbed by convection. Averaging times also noted.

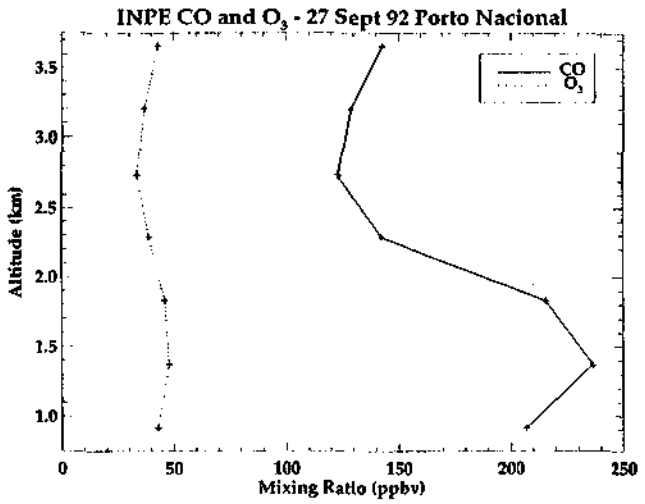

Figure 7. Profiles of CO (ppbv) and O_3 (ppbv) taken from INPE aircraft on September 27, 1992, near latitude −10°, longitude −54°.

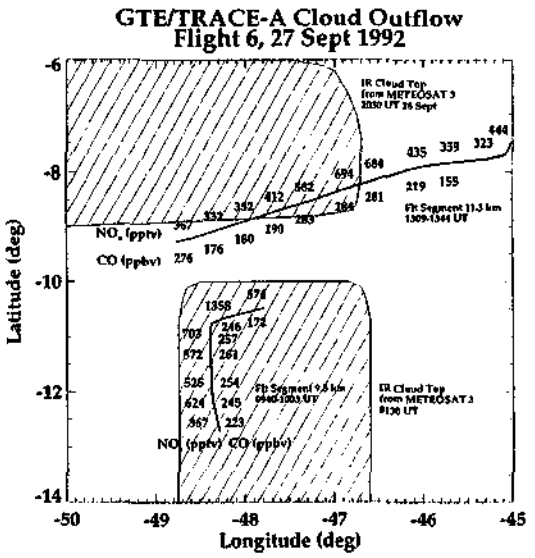

Figure 8. TRACE A flight 6 constant-altitude measurements of CO and NO_x in cloud-processed air at 9.5 and 11.3 km. Approximate locations of cold cloud tops sketched from Meteosat 3 imagery received in the field for indicated times, which are approximate times of peak system development.

3.2. Observations in Cloud-Processed Air

3.2.1. Description of measurements. The primary segments of flight 6 with cloud-processed air are the portion of descent 2 from 11.3 to 5 km and portions of constant-altitude segments 1 and 9 (9.5 km) and segment 5 (11.3 km). Measurements of CO and NO_x for constant-altitude segments 1 and 5 in cloud-processed air are shown in Figure 8. CO at 9.5 km was remarkably uniform at 240–260 ppbv over a 15-min period of flight through a region that satellite imagery from 8 to 9 hours earlier shows to be covered with a large anvil from convective storms (the second and more southerly system described in section 2). High CO values were found during the 11.3-km flight leg due to the more northerly convective system; 5-s average values reached 340 ppbv and three consecutive 3-minute averages exceeded 280 ppbv. These mixing ratios exceed all upper tropospheric cloud outflow CO measurements previously reported in the literature [e.g., *Dickerson et al.*, 1987; *Luke et al.* 1992]. CO mixing ratios remained between 200 and 300 ppbv for most of the descent from 11.3 to 5 km. On the 9.5-km flight segment, very high NO_x mixing ratios exceeding 1300 pptv (3-min average) were found. Several 3-min averages at 11.3 km are in the 500–700 pptv range. In contrast to these measurements are mixing ratios of NO_x in relatively undisturbed air of 150–200 pptv.

Ozone mixing ratios may be slightly depressed in the cloud-processed air compared with those in air undisturbed by the storms. At 9.5 km the values are in the 59–68 ppbv range, compared with 72–78 ppbv in undisturbed conditions. At 11.3 km there is negligible difference (76–82 ppbv O_3 in the cloud-processed air versus ~80 ppbv in undisturbed air). These measurements were taken at 1015–1045 LT, and photochemical O_3 production may already have compensated for any dilution of ozone caused by upward transport of lower O_3 mixing ratios from below. The 9.5 km measurements were made too early in the morning (0640–0703 LT) for much O_3 to have been produced and therefore reflect the effects of dilution.

Three samples were taken for hydrocarbon analysis in the cloud-processed air at 9.5 km, and five samples were analyzed from the 11.3-km level. Sample duration varied from 63 to 111 s. Two samples at 9.5 km and three at 11.3 km showed total NMHC to be in the 7–9 ppbv C range, while total NMHC in undisturbed air at these altitudes was 2–4 ppbv C.

Further evidence of cloud processing comes from the altitude variation of the hydroperoxide ratio, H_2O_2/CH_3OOH, observed on flight 6 (Figure 9a). In the region of recent deep convection, hydroperoxide ratios less then 1 were encountered at high altitudes (9.5 and 11.3 km). Photochemical model-simulated ratios of H_2O_2 to CH_3OOH [e.g., *Jacob et al.*, this issue] indicate expected values always exceeding 1 and generally greater than 2 in the absence of vertical transport, precipitation, and in-cloud reactions. The hydroperoxides were used by *Heikes et al.* [1996] to identify air samples at an altitude which may have been recently processed by cloud or precipitation. Air transported from low altitude will contain anomalously high concentrations of CH_3OOH compared with more typical concentrations of CH_3OOH at the same altitude. H_2O_2 concentrations may or may not be elevated depending upon whether precipitation occurred during convective lifting or whether sulfur dioxide was present during vertical transport in cloud. Precipitation will reduce H_2O_2 relative to CH_3OOH because of the significantly greater solubility of H_2O_2 compared to that of CH_3OOH [*O'Sullivan et al.*, 1995]. Sulfur dioxide will react with H_2O_2 in cloud water at a rate greater than that for CH_3OOH. Although not measured on TRACE A, SO_2 mixing ratios are expected to be small over the cerrado of Brazil due to minimal fossil fuel burning. Therefore precipitation scavenging is expected to be the primary factor causing the small values of the H_2O_2 to CH_3OOH ratio found in the upper troposphere during flight 6. In contrast, Figure 9b shows the altitude variation of the hydroperoxide ratio for flight 7, the Brazilian biomass fire characterization flight. All ratio values are >1 and only a few are <2, reflecting minimal influence of recent cloud processing.

3.2.2. Evidence of lightning contributions to observed NO_x. High NO_x mixing ratios are more patchy than CO measurements in cloud-processed air, particularly at 9.5 kin (Figure 8). For 12 of 17 3-min periods on constant-altitude flight segment

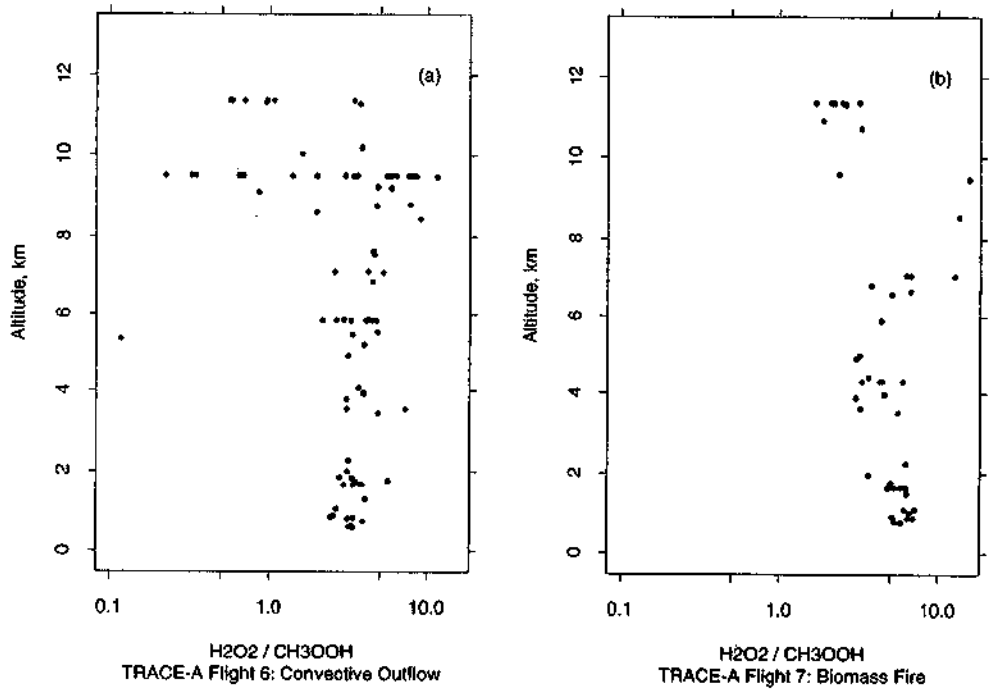

Figure 9. Measured ratio of H_2O_2 to CH_3OOH versus altitude for TRACE A flights (a) 6 and (b) 7.

1, the ratio (pptv NO_y/ppbv CO) was in the range 1.65–2.09 with a mean of 1.93; the ratio was well above this range for the remaining five 3-min periods (see Table 1). We use these ratios to estimate the recent NO_y contribution from lightning. We assume no lightning contributions for the points having ratios in the "normal" range but note that these points could be enriched by lightning NO_y from storms farther upstream.

First, we estimate the amount of NO_y at each point that would be present if there were no lightning by multiplying the measured [CO] by the mean ratio in air with no lightning effects (1.93). We then subtract the "no lightning NO_y" from the measured NO_y to obtain the lightning NO_y (Table 1). For the 9.5 km altitude the lightning contributions range from 150 to >800 pptv. For the 11.3-km flight leg 8 of the 10 3-min periods have NO_y/CO ratio values in the 1.89–2.44 range with a mean of 2.14; for the remaining two points we estimate lightning NO_y contributions to be between 101 and 128 pptv. For the points in Table 1, at least 40% of the measured NO_y is due to recent lightning at 9.5 km and at least 32% is contributed by lightning at 11.3 km. *Smyth et al.* [this issue] suggest that lightning is a major contributor to the pervasively high NO_y mixing ratios measured in the upper troposphere during TRACE A.

4. Mesoscale and Cloud-Scale Model Simulations of September 26–27 Convective Systems

Measurements in cloud-processed air were conducted only over sampling ranges of 300–400 km, which are smaller than the scale of the convective systems operating during the overall episode. Therefore we use a mesoscale model (MM5) to examine the regional impact of convection on trace gas distributions. The simulation procedure consists of running the mesoscale meteorological model [see *Wang et al.*, this issue], storing the computed wind fields, and using them in an off-line tracer transport model. We transport CO because of its relatively long lifetime (~1 month) in the troposphere. We have

Table 1. Estimation of NO_y From Lightning

Time, UT	NO_y/CO	CO, ppbv	NO_y pptv		Lightning NO_y
			Measured	No Lightning	
		9.5 km			
0943:28	2.54	245	624	473	151
0950:28	3.34	261	872*	504	368
0953:28	2.70	257	694*	496	198
0956:28	5.52	246	1358*	474	884
1000:28	3.35	172	574	331	243
		11.3 km			
1308:59	4.30	161	445	344	101
1311:59	3.56	91	323	194	128

Times are beginning times for 3-min averages. Values with asterisk indicate that NO_2 detection limit value (~230 pptv for these time periods) used for the NO_2 component of NO_y.

also performed a detailed simulation of one convective cell from the more southerly convective system using winds from the three-dimensional GCE model to transport CO, O_3, NO_y, and total NMHC. In section 4.1 we derive initial conditions from the trace gas measurements and fire count data for the regional CO tracer simulation and the cloud-scale tracer studies. Section 4.2 describes the cloud model simulation and the cloud-scale tracer transport results. Section 4.3 presents the results of the regional-scale CO transport calculations using the MM5 fields. The regional CO distribution in cloud-processed air is the basis for initializing forward trajectories to determine longer-range transport of cloud outflow (see section 5) and areas of the South Atlantic basin where O_3 produced in the outflow would be found.

4.1. Initial Conditions for Tracer Studies

Lacking detailed CO emission data, we rely on the aircraft CO measurements to develop initial conditions for model tracer simulations. The DC-8 CO profile measurements in very polluted air and relatively clean air in the lower troposphere (e.g., Figure 5) and constant-altitude flight leg averages (Figure 6) are used to construct initial condition CO profiles (Figure 10) for "polluted" air, "semipolluted" air, and "clean" air. The "semipolluted" profile is based on the INPE aircraft profile (Figure 7) taken in moderately polluted air.

The daily gridded fire counts are used to distribute the three CO profiles (Figure 11) The "polluted" profile is assigned to regions with major concentrations of fires noted on the September 26 fire map. Major areas of fires noted on the September 25 fire map and not also appearing in the September 26 data were assigned the "semipolluted" profile. Remaining areas in the MM5 fine mesh domain were designated as "clean." Uncertainties in this assignment include probable bias toward lower than actual mixing ratios and toward a polluted region that is smaller than what may have existed. For example, some

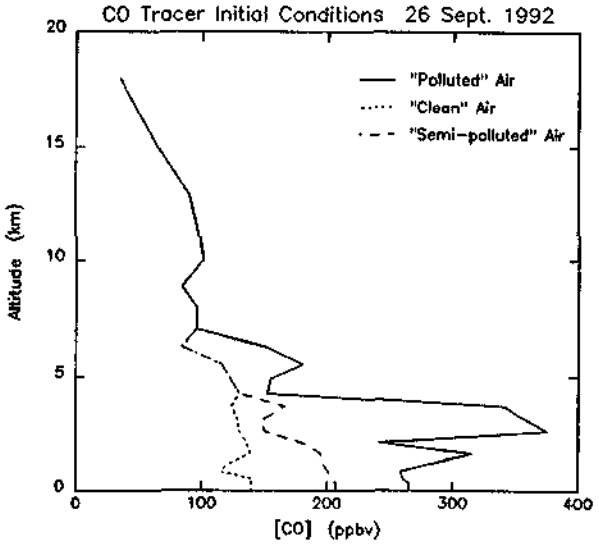

Figure 10. CO tracer initial conditions based on DC-8 flight 6 and INPE aircraft measurements. The "polluted" air profile comes from DC-8 ascents 1 and 3, descent 2, and the constant-altitude segments 3 and 6. The "clean" air profile is derived from ascent 4, descents 1 and 3, and constant-altitude segments 2 and 8. "Semipolluted" profile comes from INPE aircraft measurements.

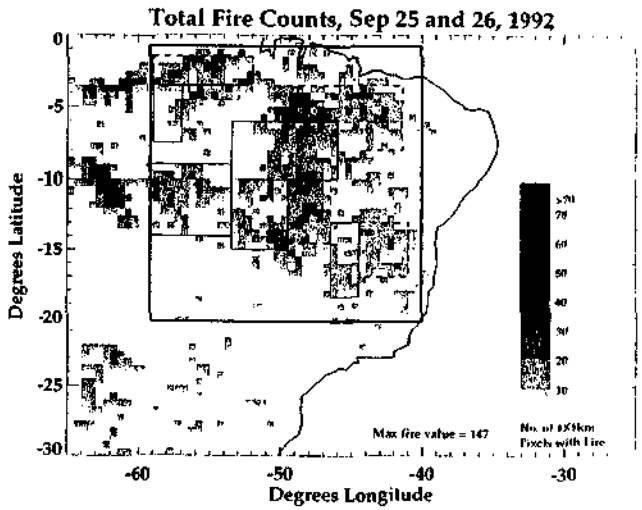

Figure 11. Combined AVHRR fire counts for September 25–26, 1992, from Justice et al. algorithm. Geographic distribution of regions designated as containing "polluted" (dashed line boxes), "semipolluted" (solid line boxes), and "clean" (remaining area) air.

of the areas for which we use the "clean" profile were probably polluted by low-level transport from fire-rich areas. In addition, even the "polluted" profile is based on data from polluted layers already 12–24 hours old.

Initial conditions for the cloud-scale tracer simulation assume the convective cell formed over a polluted region because the more southerly convective system developed over a fire-rich region on September 26. The "polluted" CO profile (Figure 10) is used for initially undisturbed conditions along with NO_y, O_3, and total NMHC profiles derived from the same flight segments used in developing the CO profile (see Table 2).

4.2. Cloud-Resolving Model Simulation of September 26–27 Convective Cell

The MM5 simulation completes the CO picture for which cloud outflow measurements were restricted to 300- to 400-km flight segments at 9.5 and 11.3 km. For the vertical structure of other trace gases required in photochemical calculations we turn to the cloud-resolving model. The three-dimensional GCE model is used to simulate one representative convective cell from the more southerly of the two major convective systems of the September 26–27 episode. Details of the model can be found in the work of *Tao and Simpson* [1993].

The initial sounding used in the GCE model simulation is selected from the MM5 mesoscale model output [*Wang et al.*, this issue] at 1930 UT September 26 at 14°S, 49°W), which is in the region where the second and more southerly convective system developed. The GCE model shows an intense convective cell growing to a height of about 16 km, in good agreement with the satellite imagery. At 180 min into the simulation the cell began to dissipate. We ran the tracer transport calculations from the initiation of the cell through the 180-min mark. When we compare the average DC-8 observations at 9.5 and 11.3 km with calculated values averaged over the distance (~40 km) covered by the DC-8 during 3 min, the simulated CO and NO_y mixing ratios are too low. Simulated O_3 was slightly greater than observed in cloud-processed air at 9.5 km; the simulated total NMHC was comparable to the measurements. As de-

Table 2. Initial Conditions for GCE Tracer Simulation

Altitudes, km	CO, ppbv	NO_x, pptv	O_3, ppbv	Total NMHC, ppbv C
0.00–1.05	260	490	49	12.8
1.05–1.73	310	295	49	13.9
1.73–2.53	223	156	49	10.4
2.53–3.92	359	323	72	13.1
3.92–4.99	153	102	60	4.1
4.99–6.16	182	112	77	4.7
6.16–7.44	147	100	74	2.5
7.44–8.12	89	126	70	2.6
8.12–8.83	95	177	74	3.1
8.83–12.78	95	208	76	3.6
12.78–16.42	90	310	100	2.5
>16.42	30	500	150	0.5

scribed in section 4.1 we have reason to believe that the initial CO and NO_x mixing ratios are too low. Therefore we adjusted the initial condition values of CO and NO_x in the polluted layers of the lower troposphere such that the model more closely matched the observations (measured CO and our estimated "No lightning NO_x" (Table 1)) at the cloud outflow sampling altitudes. This process required a factor of 1.3 for CO and a factor of 1.8 for NO_x. We also adjusted low-level O_3 values by a factor of 0.85, so that the upper level O_3 matched the measurements. Apparently, the NMHC measurements (based on grab samples) in the polluted layers were representative of conditions before the storm. Plate 2 shows the final cloud-scale simulation tracer results for the 9.5-km level. CO in the core updraft region of the storm exceeds 250 ppbv and the area perturbed by the cell is ~100 km in horizontal dimension. Lower O_3 from the boundary layer appears in the updraft region at 9.5 km, whereas downdrafts at the outer edges of the cell bring higher O_3 downward. At 11 km a region covering a distance of ~100 km in the cloud-scale simulation has ~65 ppbv O_3. Measurements made in cloud-processed air at 11.3 km 4–5 hours after sunrise are >75 ppbv, showing that appreciable O_3 production had already taken place in the cloud outflow. Table 3 presents statistics from the simulation for the 9.5-, 11-, and 14-km levels (the latter used in upper tropospheric photochemical model calculations of O_3 production (see section 5.2)).

4.3. Regional CO Transport

The three-dimensional wind fields from the MM5 simulation were used in a tracer transport code containing a positive-definite advection scheme (see details by *Wang et al.* [this issue]). Vertical transport is achieved using grid-scale (30 km horizontal resolution) winds plus the subgrid convective transport information provided from the cumulus parameterization in MM5. The regional tracer transport simulation was initialized at 1200 UT September 26 with the CO mixing ratio distribution described in section 4.1. However, the CO initial values on the "polluted" and "semipolluted" profiles were adjusted in the lower troposphere in the same manner as in the cloud-scale tracer simulation (factor of 1.3) to estimate mixing ratios for the lower troposphere that may have existed at the onset of convection. MM5 simulations were conducted with the Grell and Kain-Fritsch cumulus parameterizations, and tracer transport calculations using the output of both schemes are reported by *Wang et al.* [this issue]. Tracer simulations using the Grell scheme produced a slightly better representation of the mean and frequency distribution of the CO measurements, particularly at 11.3 km. Therefore in this paper we use only the tracer transport calculations resulting from the use of the Grell scheme.

Plate 3 presents the simulated distributions of CO at altitudes 9.5 and 11 km at 1200 UT September 27. A region of >1500 km in horizontal dimension has been perturbed at these altitudes by the two convective systems; this is about 6 hours after dissipation of the second, more southerly system, and about midway between the DC-8 sampling times at 9.5 and 11.3 km. With very light upper level winds, CO peaks in the vicinities of individual storms still persist. CO perturbations extend to the top of the cloud at approximately 16 km, having tapered off in horizontal dimension above 12 km to only 400 km at 16 km altitude. The cloud-perturbed region is also

Table 3. Statistics From Cloud-Scale Tracer Simulation

	CO, ppbv	NO_x, pptv	O_3, ppbv	Total NMHC, ppbv C
		9.5 km		
Maximum	294	407	85	9.5
Minimum	95	208	59	3.6
120-km average	182	280	72	6.0
		11 km		
Maximum	340	450	85	10.6
Minimum	95	216	59	3.5
120-km average	243	361	64	8.0
		14 km		
Maximum	254	495	108	8.5
Minimum	90	315	70	2.5
120-km average	165	368	87	5.3

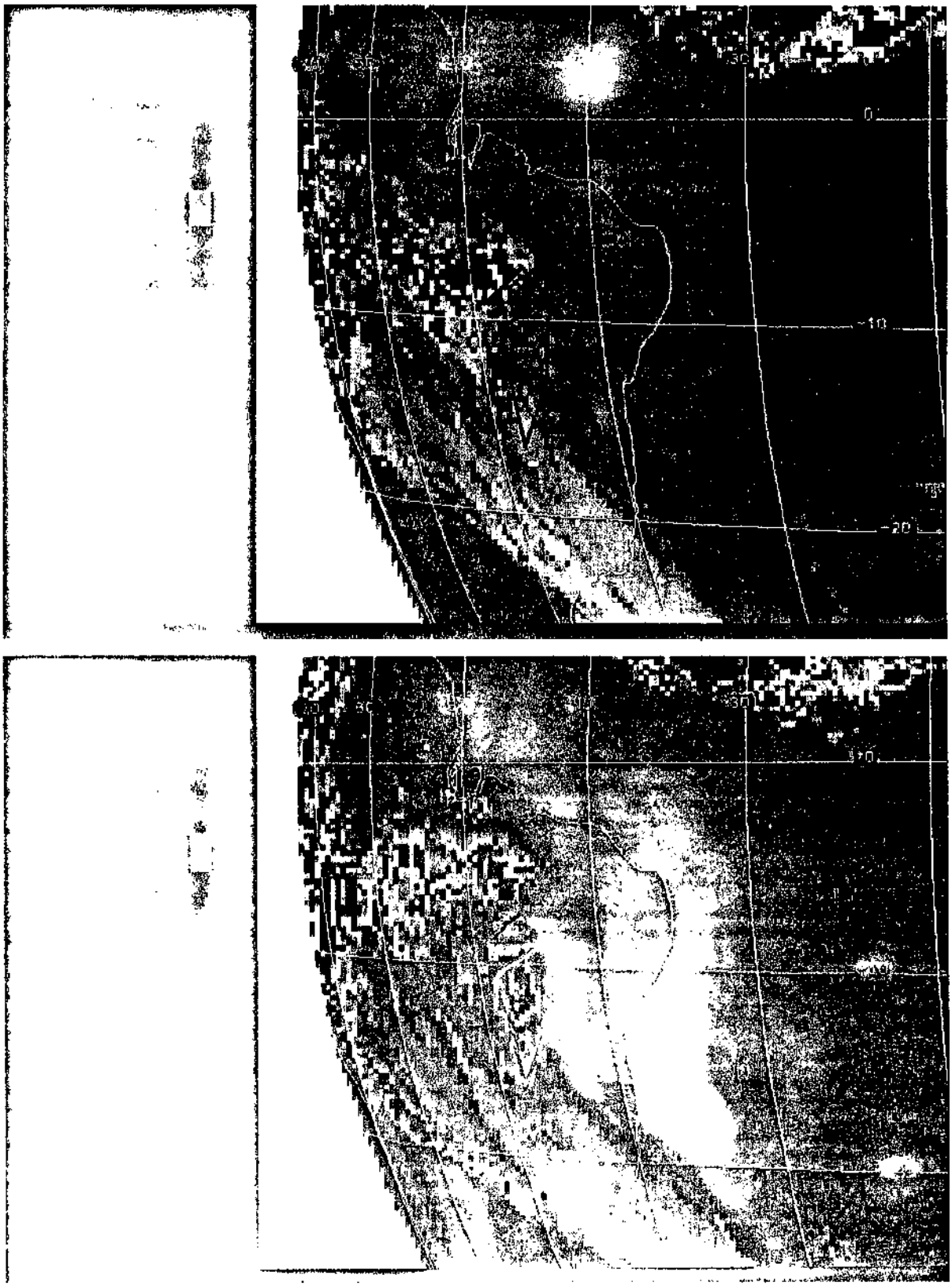

Plate 1. Meteosat 4 imagery from (a) 1830 UT September 26 and (b) 0330 UT September 27, 1992. Approximate flight track for TRACE A flight 6 of the NASA DC-8 is shown with solid line. INPE aircraft sampled in the vicinity of 10°S 54°W.

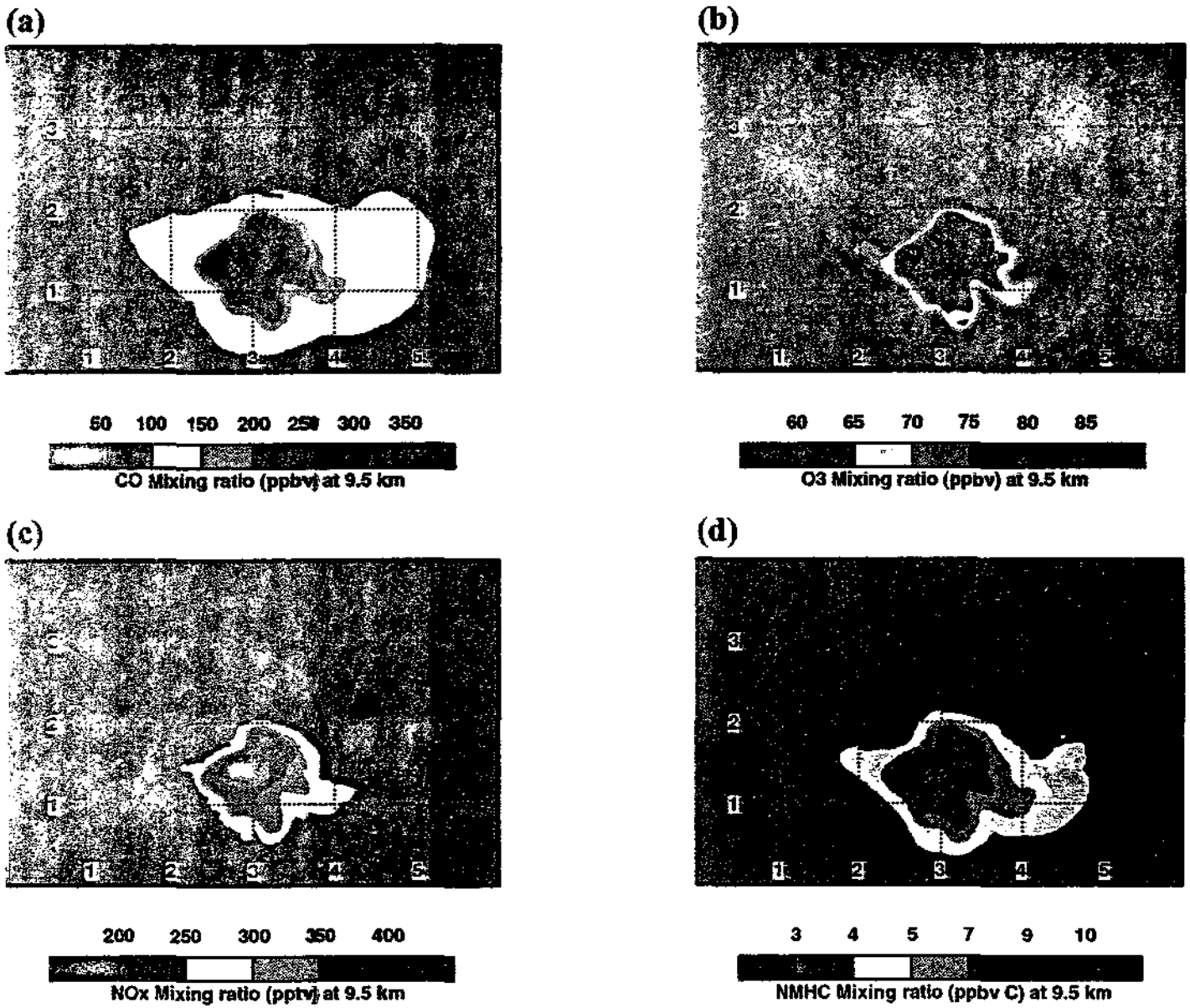

Plate 2. Maps of tracer simulation results using three-dimensional GCE wind fields. (a) CO; (b) O_3; (c) NO_x; (d) total NMHC at 180 min for altitude 9.5 km. Grid spacing is 2 km in the x and y directions in the central part of the model domain (the region shown) having 96 × 64 grid points. Grid lines are drawn every 32 km (16 grid cells). A stretched vertical coordinate (height increments from 220 to 1050 m) with 32 grid points is used to maximize resolution in the lowest levels of the model. The model top is at about 21 km.

MM5 Simulation of System Sampled on GTE/TRACE-A

Positive definite scheme, grid+subgrid transport

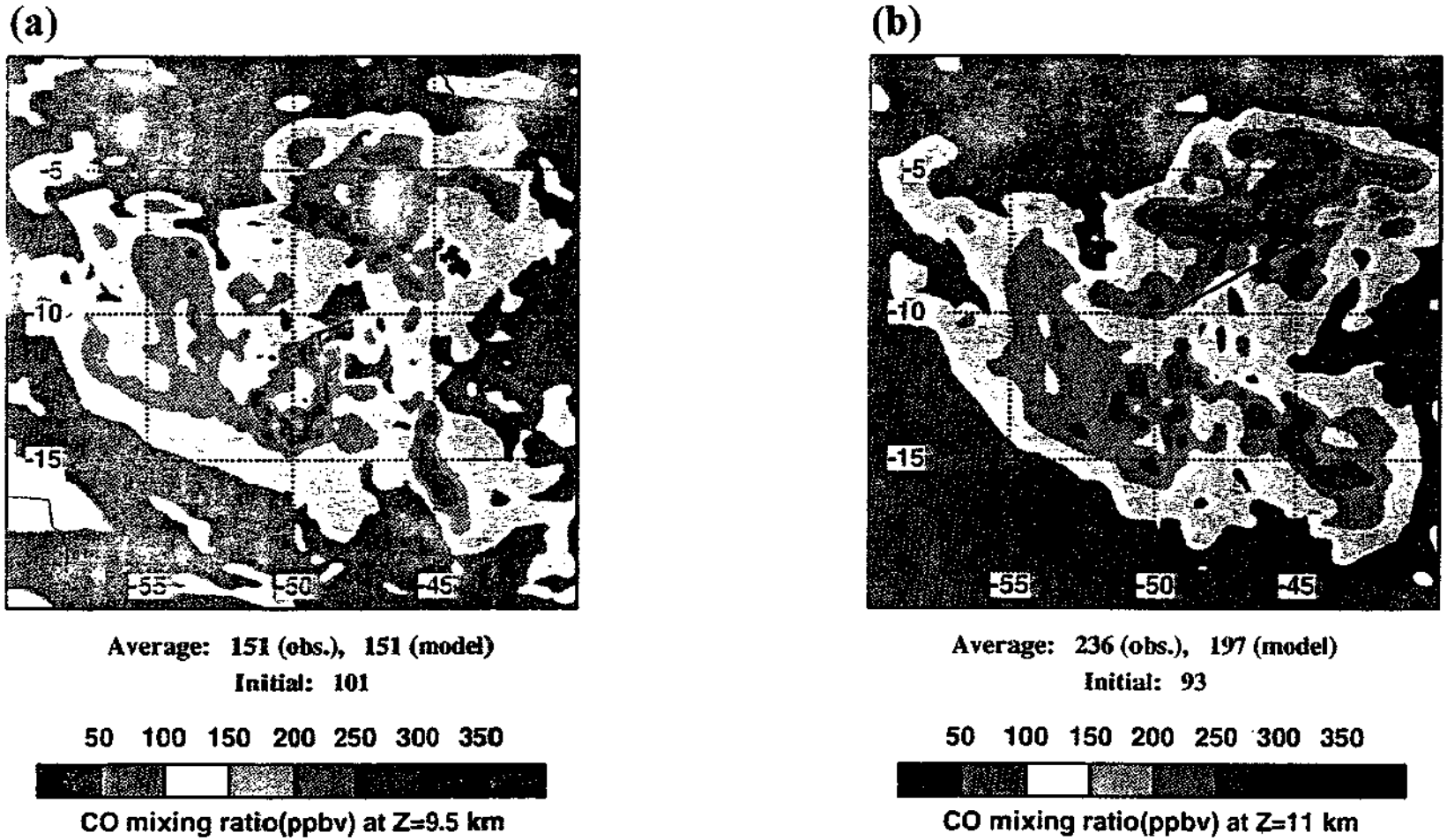

Plate 3. MM5 simulation results for CO tracer. Mixing ratios at 1200 UT September 27 at altitudes (a) 9.5 km and (b) 11 km. Region shown is fine-grid domain of MM5 simulation (30-km resolution). Includes grid-scale and subgrid transport.

Table 4. Statistics From Regional CO Simulation

	10°–15°S 48°–52°W			6.5°–10°S 44°–49°W		
Altitude, km	Max.	Min.	Avg.	Max.	Min.	Avg.
8	263	85	118	331	88	147
8.5	256	80	125	331	90	154
9	281	84	139	319	91	161
9.5	302	89	152	323	94	170
10	291	91	159	350	94	180
10.5	302	90	164	357	89	191
11	307	99	169	353	93	197
11.5	290	101	173	315	94	187
12	336	100	179	314	95	173
12.5	379	84	183	271	92	150
13	350	78	181	234	85	126
13.5	374	74	174	205	77	110
14	359	71	162	151	70	94
14.5	340	61	148	109	59	77
15	328	56	130	78	54	63
			3-min Average Observations			
9.5	261	80	151			
11.3				284	91	236

smaller at altitudes less than 9.5 km. Table 4 presents statistics from the regional CO simulation at altitudes ranging from 8 to 15 km for regions surrounding the 9.5- and 11.3-km DC-8 flight track segments (shown on Plate 3). Peak (30 km horizontal resolution) CO mixing ratios exceed 300 ppbv up through 15 km in the 10°–15°S and 48°–52°W region but are smaller above 12 km in the more northerly region. It appears that convective transport was more vigorous in the more southerly convective system. The altitude of greatest CO (both average and local maximum) in the cloud outflow was 11 km for the more northerly system and 12.5 km for the more southerly system. Table 4 also contains statistics for the 3-min average CO measurements at 9.5 and 11.3 km. Our regional simulation estimate of the average value at 9.5 km in the more southerly region (152 ppbv) compares very well with the average observed value (151 ppbv) at this altitude. The mean of the simulated CO in the more northerly region at 11 km (197 ppbv) is somewhat lower than the mean of the observations in this region (236 ppbv).

We also compare the model-simulated CO mixing ratios with the measurements in cloud-processed air at 9.5 and 11.3 km by means of frequency distributions (see Figures 12a and 12b). Observations are compared with simulated values from regions surrounding the flight track measurements (same regions as in Table 4), although the comparison is not strictly on a one-to-one basis because the simulated clouds are slightly displaced relative to the observed clouds. At both altitudes the observed frequency distributions show a double peak, whereas the simulated CO distributions show only single peaks. Otherwise, the frequency distribution of the simulated values compares well with that of the observations at 11.3 km. At 9.5 km the comparison is not so good; the simulated distribution does not show enough low CO mixing ratios. Differences in the distributions may be due to inadequacies in the simulation or sampling area. However, we are encouraged by how well the model simulates the mean values over the subregions. Simulated CO distributions in the 8- to 16-km layer are used to initialize forward trajectories to demonstrate the long-range transport of O_3-producing convective outflow over the South Atlantic basin.

5. Long-Range Transport and Photochemical Simulations

The cloud outflow observed on TRACE A flight 6 is transported downstream by upper tropospheric winds. We use the GSFC isentropic trajectory model to compute forward trajectories (section 5.1) from the cloud outflow measurement locations and from the enhanced CO region in the MM5 simulation. We estimate the amount of ozone produced during this transport with a photochemical box model (section 5.2) and compare the results with downstream measurements (e.g., ozonesondes at Natal) in section 5.3.

5.1. Forward Trajectories From Convective Outflow

We computed forward trajectories (Figure 13) from selected points on the DC-8 flight track in the convective outflow at 9.5 and 11.3 km. The trajectories were computed for clusters about the points of interest and using the European Center for Medium-Range Weather Forecasts (ECMWF) and National Meteorological Center (NMC) global analyses (as recommended by *Pickering et al.* [this issue]). The trajectories show that the measured cloud outflow at 11.3 km (Figures 13a and 13b; theta = 348.6 K) was transported in the westerlies over northeastern Brazil and across the South Atlantic to the coast of Africa in 8 days. The NMC trajectories show a straighter west to east flow, whereas the ECMWF trajectories show a higher-amplitude wave pattern. Trajectories with both sets of input analyses show very low wind shear in the horizontal, illustrated by the clusters remaining cohesive for the 8 days. At 9.5 km (Figures 13c and 13d; theta = 342.7 K) the initial transport is to the southeast based on the NMC analyses and to the northeast based on the ECMWF data. The trajectories cross over the mid-Atlantic, both clusters arriving near the African coast in 8 days. The horizontal shear at this level is considerably greater than at 11.3 km, evidenced by a greater spread within the clusters.

A systematic analysis is carried out by initiating 8-day forward isentropic trajectories in two layers (8–12 and 12–16 km) from points shown by the regional tracer simulation to be most

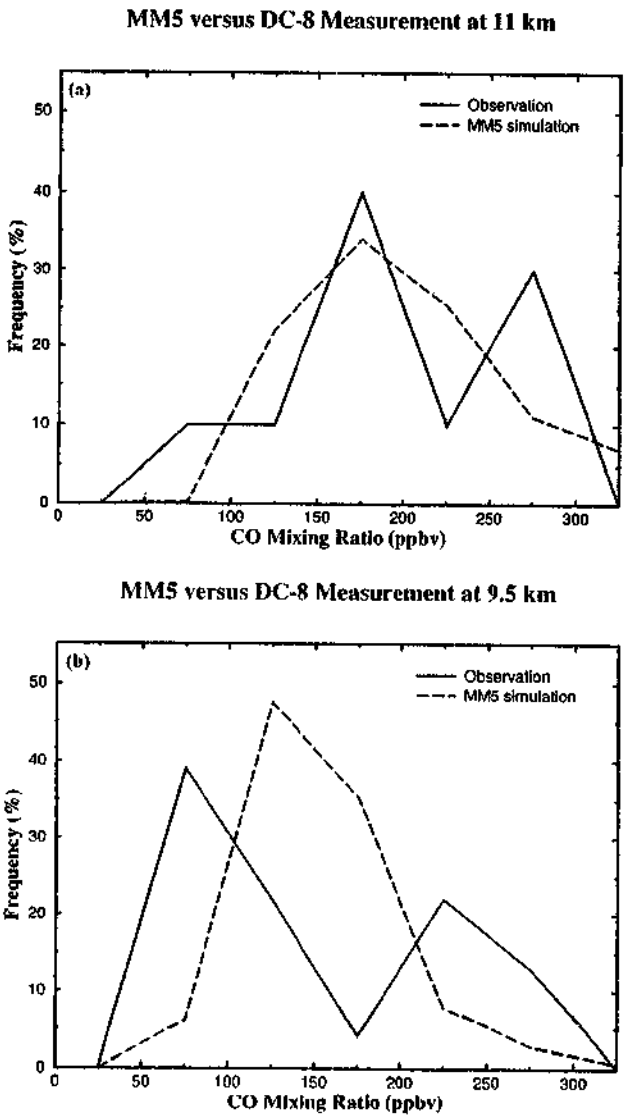

Figure 12. Frequency distributions of CO measurements and MM5-simulated values in indicated regions and altitudes (a) 6.5°–10°S, 44°–49°W at 11.3 km; (b) 10°–15°S, 48°–52°W at 9.5 km. Mixing ratios from MM5 tracer calculation are 30 km grid resolution values, while the measurements from the DC-8 are 3-min averages (equivalent to approximately 40-km travel distance).

CO-perturbed. For the 8- to 12-km layer, trajectories are run on isentropic surfaces representative of 8, 10, and 12 km from points at these altitudes with simulated CO greater than 150 ppbv. For the 12- to 16-km layer we ran trajectories on isentropic surfaces representative of 12, 14, and 16 km from points with the same criterion value. In both layers, trajectories from points with CO >250 ppbv were differentiated from those with CO between 150 and 250 ppbv. Figure 14 shows the positions of these trajectories at 4 and 8 days downstream. In the 8- to 12-km layer, air parcel positions at 4 days downstream are clustered over northeast Brazil and the western South Atlantic. By 8 days, parcel locations stretch from northeast Brazil to the vicinity of Australia. Clusters of parcels initially containing >250 ppbv CO were near the northeast Brazilian coast, off the coast of Angola, and in the Mozambique/Madagascar region. In the 12- to 16-km layer, parcels at 4 days are tightly clustered in the western South Atlantic with many of them reaching Africa by 8 days. This analysis suggests that Brazilian convective outflow sampled on September 27 can affect upper tropospheric ozone over widespread regions of the Atlantic, Africa, and the Indian Ocean. Furthermore, parcels with heavily polluted air (parcels initially with >250 ppbv CO) are distributed throughout the affected area.

5.2. Photochemical Box Model Simulations of O_3 Production

A time-dependent photochemical box model is used to compute trace gas concentrations and net O_3 production during the 8-day transport described in section 5.1. The model uses the same chemical mechanisms as the GSFC point model described by *Thompson et al.* [this issue]. A 15-min time step is used, except that a 1-s time step is used near the day-night transitions. Clear-sky photolysis rates are assumed.

Box model simulations for conditions in the 8- to 12-km and 12- to 16-km layers (4-km mixing depth) are initialized with measured or cloud model-simulated mixing ratios of selected species. For the 8- to 12-km layer the model is initialized with cloud-processed constituent measurements at 9.5 and 11.3 km and undisturbed conditions at 9.5 km (Table 5). Net ozone production is calculated for four conditions: (1) undisturbed; (2) mixing ratios averaged over all cloud-processed air; (3) peak 9-min average (~120 km) cloud-processed mixing ratios at 9.5 km; and (4) peak 9-min average cloud-processed mixing ratios at 11.3 km. For the 12–16 km layer we use the cloud-scale tracer transport results for 14 km (undisturbed conditions and peak 120-km average mixing ratios in cloud-processed air; see Table 6).

Figure 15 summarizes net ozone production rates in the two cloud outflow layers. Peak values of O_3 production in the first four days downstream from the convective region are 24–27 ppbv in the 8- to 12-km layer (for cloud outflow containing ~650–950 pptv NO_x). During days 5–8 an additional 15–22 ppbv are produced; peak total O_3 production over the eight days of transport is 42–45 ppbv. This result is a factor of ~3.5 greater than the 13 ppbv O_3 produced in 8 days in undisturbed air in this layer. Peak ozone production rates for cloud outflow in this layer are initially 7–8 ppbv/d. These rates are slightly higher than those obtained for the flight 6 cloud outflow by *Thompson et al.* [this issue] and *Jacob et al.* [this issue] with instantaneous point models. The reason for this difference is that cloud outflow measurements were made only in the early to midmorning; when these instantaneous O_3 production rates are extrapolated to a 24-hour period, lower diurnal average rates are obtained than are calculated with our time-dependent box model.

In the 12- to 16-km layer, O_3 production is enhanced by a factor of ~1.7 (15.5 ppbv in 8 days in cloud-processed air versus 9 ppbv in undisturbed air). However, because there were no measurements in this layer and we use only the mixing ratios obtained from GCE model transport calculations, the box model simulation at 14 km does not include the effects of lightning on NO_x. Therefore the O_3 production rate in cloud-processed air could be greater than what we have calculated for the 12- to 16-km layer.

We have integrated the O_3 production over the 8- to 12-km and 12- to 16-km layers and these values (in Dobson units) appear in Figure 15. Peak cloud outflow contains at least 6.7 DU at the end of 8 days in the 8- to 16-km layer. Compared with the 2.2 DU produced in undisturbed air, this represents an

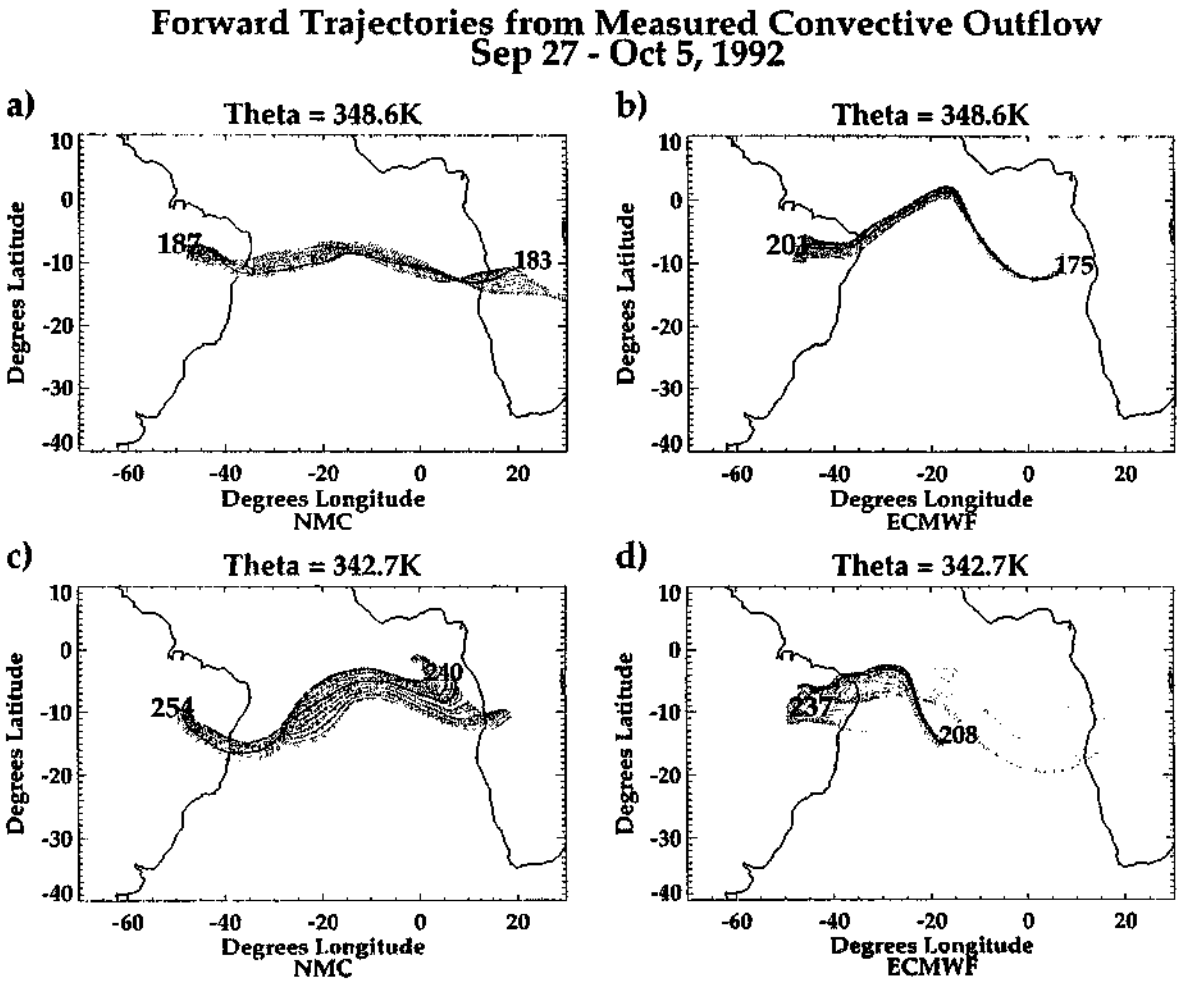

Figure 13. Forward trajectories from points on flight 6 flight track in cloud outflow: (a) from 11.3 km with NMC input; (b) from 11.3 km with ECMWF input; (c) from 9.5 km with NMC input; (d) from 9.5 km with ECMWF input. Trajectories shown with solid line with positions noted every 12 hours. Thin dashed lines are trajectories initialized in 2.5° × 2.5° cluster surrounding central point.

enhancement of at least a factor of 3. Excess tropospheric O_3 over the South Atlantic is 15–25 DU in the biomass burning season as seen from satellite and ozonesondes [*Fishman et al.*, this issue; *Thompson et al.*, this issue]. Ozone produced in the outflow from the September 26 to 27 convective event (average of ~5 and peak of 6.7 DU) can account for at least 25% of the excess.

5.3. Comparison of Simulated O_3 Production with Downstream Observations

Figure 16 shows the cumulative net O_3 production computed by the box model at 24-hour intervals as it would be observed along the pathway of a typical upper tropospheric forward trajectory from the cloud system. The photochemical and trajectory models are not actually coupled in this simulation, but

Table 5. Initial Conditions for Box Model Simulations in 8-to 12-km Layer

	11.3 km Peak Outflow	9.5 km Peak Outflow	9.5 and 11.3 km Average Outflow	9.5 km Undisturbed
O_3, pphv	77	61	73	75
NO, pptv	405	511	266	107
NO_2, pptv	240	434	282	67
CO, pphv	286	258	251	90
C_2H_4, pphv	2.03	1.63	1.82	1.29
C_3H_6, pptv	9.3	71.3	34.6	3.9
C_4H_8, pptv	322	253	275	247
C_2H_2, pptv	463	595	506	6
TOL, pptv	1	18	11	1

Taken from steady state version of model in which fluxes are parameterized to match observations in cloud-processed air at the given altitude. Invariants include HNO_3, PAN, H_2O_2, and H_2CO, which are set to measured values. TOL, toluene.

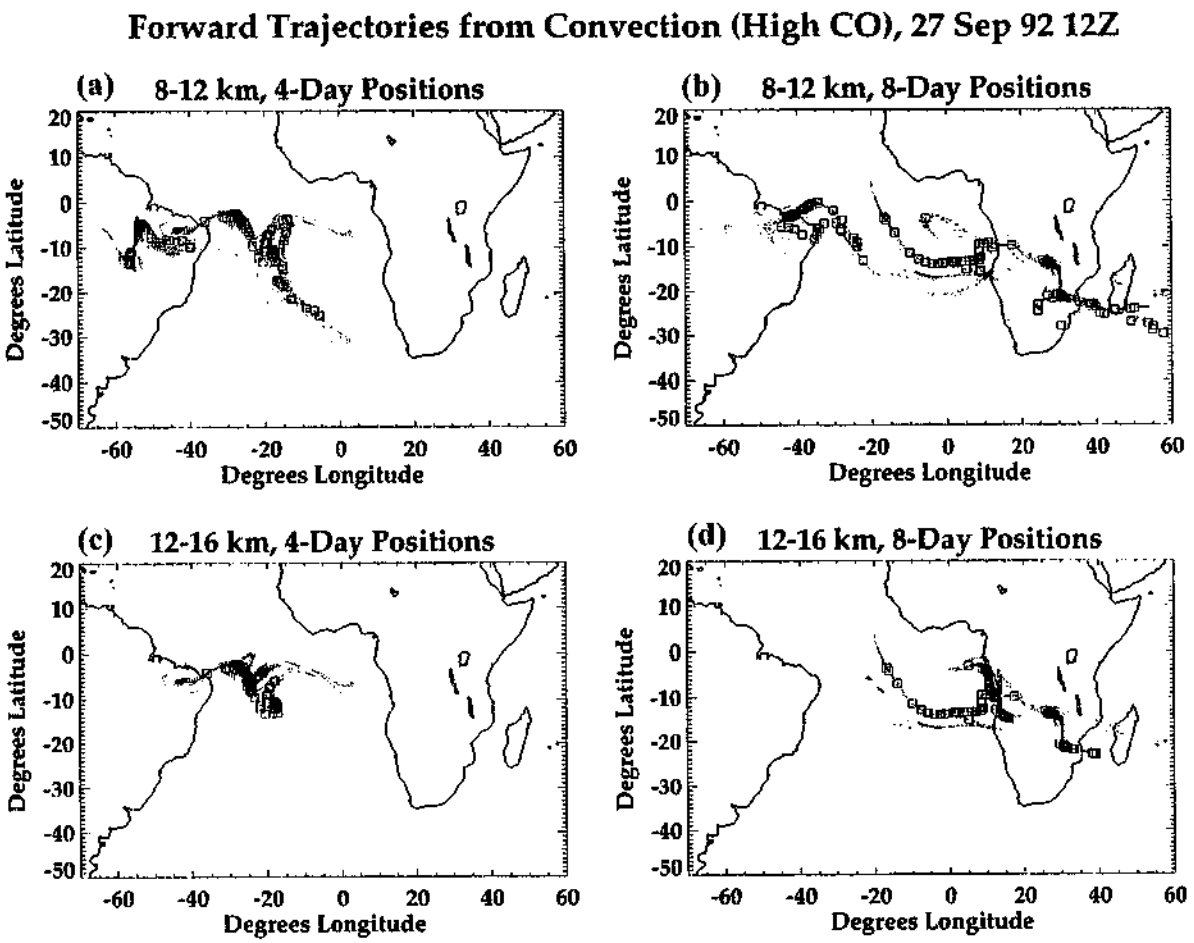

Figure 14. Parcel positions at (a) 4 days downstream and (b) 8 days downstream in the 8- to 12-km layer based on forward trajectories initialized at points on the regional CO simulation having CO >150 ppbv (Plate 3). Parcel positions in 12- to 16-km layer at (c) 4 days and (d) 8 days. Squares represent parcels having initially >250 ppbv CO, while points indicate parcels initially having 150–250 ppbv CO.

incorporation of trajectory parameters is not expected to give significantly different results. Also shown in this figure are the locations of downstream postconvection measured O_3 increments which may be compared with the simulated O_3 production amounts.

TRACE A flight 7 on September 28 (~24 hours after flight 6) sampled a region at 11.3 km about 300 km east of the center of the second and more southerly convective system of September 26–27. Ozone mixing ratios on flight 7 at this altitude averaged 88 ppbv, whereas the average on flight 6 was 78 ppbv. High CO mixing ratios (average of 210 ppbv) suggest that the flight 7 air mass contained convective outflow, although the H_2O_2/CH_3OOH ratios reach a minimum of slightly >1. Trajectories in Figure 18 suggest that 300 km is approximately the distance traveled by the convective outflow from this system in 24 hours. Therefore the DC-8 O_3 measurements show a net O_3 production rate of ~10 ppbv for the first day of downstream transport and that some H_2O_2 has been produced. Our box model calculation of 7–8 ppbv O_3 for the first day nearly matches this rate.

Ozonesonde measurements at Natal, Brazil [*Kirchhoff et al.*, this issue] show an average 31 ppbv increase in upper tropospheric (11–16 km) O_3 between September 28 and 30 (Table 7) and an average increase of 26 ppbv in the 11- to 12-km interval (Figure 16). In fact, the September 30 sounding (3–4 days after the convective episode) has the highest tropospheric ozone and the highest 12 km-to-tropopause ozone of the 14 Natal soundings in the September–October 1992 period (Figure 17). Back trajectories arriving at four levels between 11 and 16 km at Natal on September 30 (Figure 18) all show flow to Natal from the vicinity of the September 26–27 events over periods ranging from 2 to 4 days. The box model calculations show net ozone production over the first 4 days of transport to be ~24 ppbv at 11.3 km and >8 ppbv at 14 km. Thus we argue that most of the September 28–30 increase in ozone at Natal was caused by photochemical production in convective outflow from the September 26 to 27 storms.

6. Discussion

Through this case study we have shown that mesoscale convective systems over biomass burning regions of the Brazilian cerrado can cause major O_3 increases in the upper troposphere at Natal. *Thompson et al.* [this issue] have noted that Natal experienced upper level westerlies for 100% of the soundings during TRACE A, while at Ascension the frequency was 87%. These results and our forward trajectories (Figures 13 and 14) suggest that these sites are frequently downstream of the Brazilian convective outflow and that O_3 produced in the outflow may dominate the upper tropospheric O_3 distribution at these

locations. For example, the 8- to 12-km and the 12- to 16-km forward trajectories and box model O_3 production calculations show that Ascension Island could have sampled this convective outflow 4 to 6 days after the event (October 1–3) with as much as 30 ppbv of excess O_3. Upper tropospheric ozone on the October 3, 1992, sounding shows a peak of 20–30 ppbv excess O_3 at 13–15 km and other lower-altitude peaks, but no tracers were measured to allow definitive source assignment. From trajectories it appears that this feature is a combination of outflow from the September 26 to 27 cerrado storms and earlier convective events that occurred farther upstream. The effects of the September 26–27 events may reach the Brazzaville sounding location in about 8 days (Figure 14) in the 12- to 16-km layer. At the end of 8 days the box model shows net O_3 production in the 12- to 16-km layer totaling 15 ppbv. Upper level westerlies were noted for only 23% of the TRACE A soundings at Brazzaville, indicating that the potential impact we have seen at this site from the September 26 to 27 storms may be a relatively infrequent occurrence. However, none of the upper level back trajectories from individual Brazzaville soundings show flow from Brazil [*Thompson et al.*, this issue]. Because our trajectories also show flow to the Indian Ocean, particularly in the 8- to 12-km layer, the sounding site at Reunion Island could have received convective outflow from the September 26–27 Brazilian events.

Pickering et al. [1992a] estimated the amount of O_3 production during the first 24 hours following a prototype deep convective event over the Brazilian savanna during the burning season. *Chatfield and Delany* [1990] also simulated O_3 production in cloud outflow for storms over biomass burning regions of Brazil. In the *Pickering et al.* [1992a] analysis we assumed initial lower-tropospheric mixing ratios (e.g., 500 pptv NO, 450 ppbv CO) based on earlier field expeditions to Brazil during biomass burning. In the simulations with cloud dynamics based on a squall line sampled during the NASA GTE/ABLE 2A field mission over Brazil, cloud-processed air had 600–900 pptv NO_x in the 9.5- to 11-km layer, similar to the peak 9-min NO_x measured in the TRACE A flight 6 cloud outflow. An average O_3 production value in cloud outflow from 5 to 13 km was 7.4 ppbv O_3/d, with values in the 9.5- to 11-km layer of 4–5 ppbv/d.

Table 6. Initial Conditions for Box Model Simulations in 12- to 16-km Layer

	14 km	
	Peak Outflow	Undisturbed
O_3, ppbv	87.5	102
NO, pptv	293	228
NO_y, pptv	77	68
CO, ppbv	164	86
C_2H_6, ppbv	1.80	0.87
C_3H_8, pptv	5.7	2.7
C_5H_8, pptv	339	166
C_2H_4, pptv	8.1	3.8
TOL, pptv	0.9	0.4

Taken from steady state version of model in which fluxes are parameterized to match GCE model output for 14 km. Undisturbed NO_y, CO, and hydrocarbons at 14 km estimated by extrapolating 9.5 to 11.3 km trend in undisturbed mixing ratios. O_3 at 14 km taken from UV-DIAL [*Browell et al.*, this issue] measurements for this altitude. Invariants include HNO_3, PAN, H_2O_2, and H_2CO which are set to values appropriate for 14 km taken from one-dimensional model simulations discussed by *Pickering et al.* [1992a].

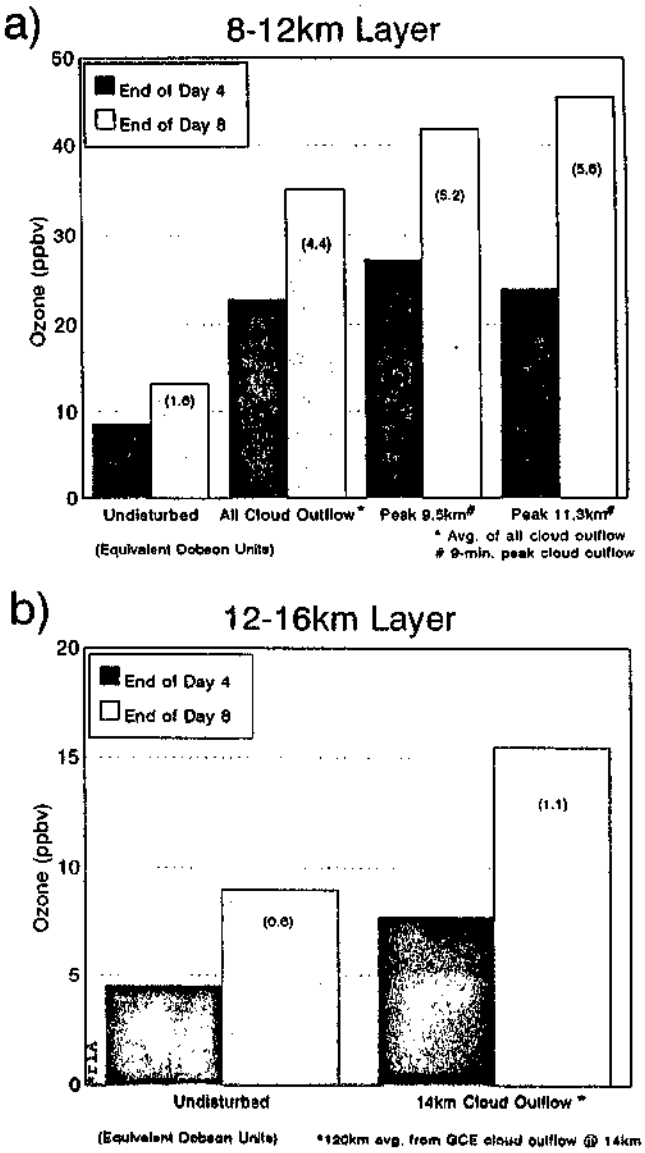

Figure 15. Summary of photochemical box model simulation (8 days) of total net O_3 production for days 1–4 and 5–8: (a) for 8-to 12-km layer and (b) for 12-to 16-km layer. Model initialized with measurements from flight 6 in 8-to 12-km layer and with output from cloud-scale simulation for 12-to 16-km layer.

Chatfield and Delany [1990] estimated 6 ppbv/d for the first 24 hours downstream of an idealized "mix-then-cook" event. These O_3 production rates are similar to those obtained from the box model using the trace gas measurements from the September 26 to 27 cloud outflow sampled on TRACE A flight 6. We have confirmed the postconvective upper tropospheric ozone enhancement predicted in our previous work and by Chatfield and Delany.

7. Summary and Conclusions

Observations in cloud-processed air following the September 26–27, 1992, convective episode over the Brazilian cerrado provide evidence of vigorous convective transport of biomass burning emissions to the upper troposphere. Enhancement of

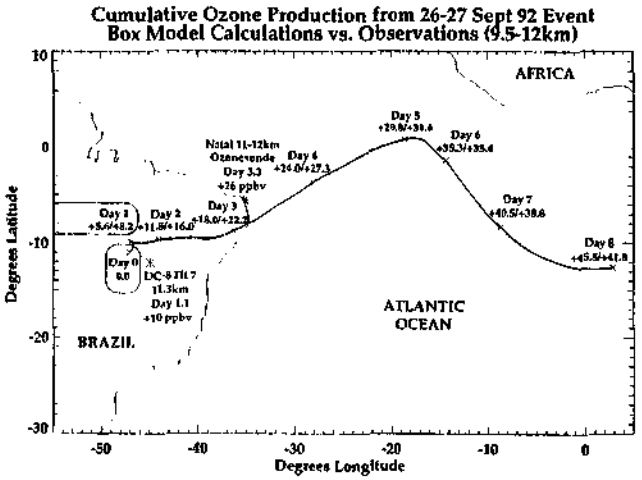

Figure 16. Cumulative net ozone production computed with Goddard tropospheric chemistry box model downstream of September 26–27, 1992, Brazilian convective systems is noted at 24-hour intervals (denoted by crosses) along a characteristic forward trajectory. The photochemical and trajectory models are not actually coupled in this simulation, but incorporation of trajectory parameters is not expected to give significantly different results. First value for each day is cumulative production using highest 9-min average cloud-outflow mixing ratios at 11.3 km (see Table 5) as initial conditions; second value is cumulative production using highest 9-min average cloud-outflow data at 9.5 km (see Table 5). Asterisks show locations of measurements; increments in measured ozone mixing ratios obtained by comparing DC-8 flights 6 and 7 data and by comparing Natal ozonesonde profiles from September 28 and 30, 1992.

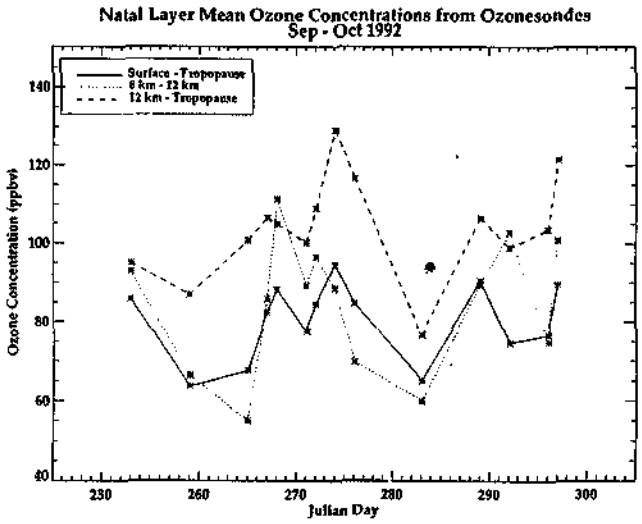

Figure 17. Layer-mean O_3 mixing ratios from Natal ozonesondes over period September–October 1992. Note high values in the 12 km to tropopause range on September 30 (day 274) and October 2 (day 276) following the major convective episode over the cerrado region.

CO mixing ratios by a factor of 3 over background values occurred in widespread convective outflow. The NO_x measured in outflow was a mixture of that transported from the lower troposphere by the convective updrafts and that produced by lightning. We estimate that the lightning contribution amounted to at least 40% of the measured NO_x mixing ratios at 9.5 km and 32% at 11.3 km in regions with a detectable lightning signature based on the NO_x/CO ratio.

Simulation of the September 26–27 convective systems with MM5 reproduces the observed features of cloud outflow and shows that at 6 hours after the decay of the two major convective systems, the perturbed CO extended over a region of 1500 km. Cloud-scale and regional-scale simulations expand the limited sampling range and show enhanced trace gas concentrations in all upper tropospheric layers extending to the cloud tops at approximately 16 km.

The regional extent of the convective systems and trajectories from sampled cloud outflow point to a significant contribution toward the South Atlantic ozone maximum. A photochemical box model, initialized with cloud outflow observations and tracer output from the GCE model, shows several parts per billion by volume O_3 per day produced as outflow is transported downstream for several days. Forward trajectories from the cloud-perturbed region show eastward

Table 7. Upper Tropospheric Ozone From Natal, Brazil, Ozonesondes

Altitude Interval, km	September 28 O_3, ppbv	September 30 O_3, ppbv	September 30–28 Delta O_3, ppbv
11.25–11.5	91.37	96.70	5.33
11.5–11.75	82.49	114.91	32.42
11.75–12.0	87.64	128.69	41.05
12.0–12.25	91.77	132.04	40.27
12.25–12.5	101.90	119.83	17.93
12.5–12.75	99.07	109.32	10.25
12.75–13.0	100.96	115.10	14.14
13.0–13.25	92.28	123.17	30.89
13.25–13.5	86.50	126.48	36.98
13.5–13.75	88.03	131.87	43.84
13.75–14.0	96.50	130.73	34.23
14.0–14.25	93.27	134.61	41.34
14.25–14.5	85.92	135.52	49.60
14.5–14.75	Msg.	130.69	Msg.
14.75–15.0	Msg.	131.0	Msg.
15.0–15.25	96.97	127.77	30.80
15.25–15.5	97.24	134.19	36.95
Mean	92.79	124.86	31.07

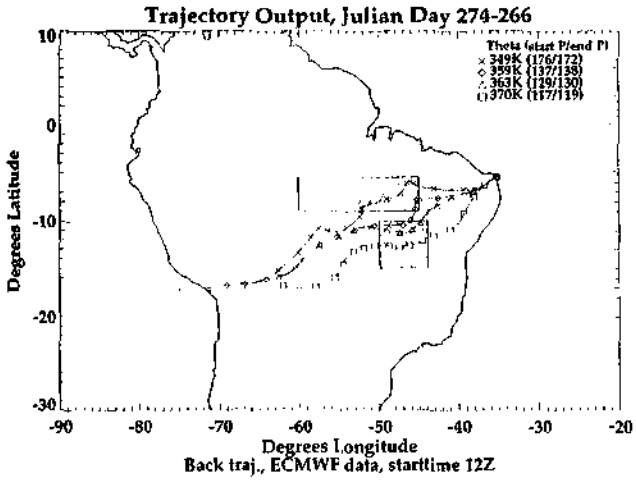

Figure 18. Backward trajectories arriving at Natal on September 30, 1992, on four potential temperature surfaces. Boxes show locations of September 26–27 convective regions.

flow from the 9.5 and 11.3 measurement altitudes across the South Atlantic and reaching Africa in 8 days. Ozone measurements on flight 7 at 11.3 km (downstream of the more southerly convective system) were ~10 ppbv higher than on flight 6, suggesting an O_3 production rate similar to our box model calculation for the first 24 hours of transport. Three days after flight 6 the September 30, 1992, ozonesonde at Natal shows an average increase of ~30 ppbv (~3 Dobson Units) in the upper troposphere compared to two days earlier. Back trajectories confirm the sounding-convection link. Air arriving at Natal on September 30 in a 5-km-deep upper tropospheric layer was transported from the convective region over the cerrado in 2–4 days. Trajectory analyses by *Thompson et al.* [this issue] show that upper tropospheric ozone in soundings at Natal, Ascension Island, and African stations (south of 15°S) throughout TRACE A was transported from South America. This paper complements that study with direct evidence of ozone forming in the upper troposphere after deep convection detrains biomass burning emissions. *Kirchhoff et al.* [this issue] show that the 1992 wet season had an early onset and middle and upper tropospheric ozone was higher than usual. This suggests that the role of deep convection in the South Atlantic regional ozone budget for the TRACE A period may have been more prominent than in a typical year.

Acknowledgments. This work was supported under the NASA Tropospheric Chemistry Program (to AMT), the NASA Physical Climate Program (to WKT), the NASA Atmospheric Effects of Aviation Program (to KEP), and an EOS Interdisciplinary Study. We thank A. Motta of INPE and L. Cavalcante, F. Diniz, and O. Chiesa of the Brazilian Departamento Nacional de Meteorologia in Brasilia for assistance during the field mission. Thanks to A. Setzer for providing weekly fire count data and to J. Kendall and C. Justice for processing daily fire counts. Thanks also to T. Kucsera for chemical modeling assistance.

References

Bachmeier, A. S., and H. E. Fuelberg, A meteorological overview of the TRACE A period, *J. Geophys. Res.*, this issue.

Browell, E. V., et al., Ozone and aerosol distributions and air mass characteristics over the South Atlantic basin during the burning season, *J. Geophys. Res.*, this issue.

Chatfield, R. B., and P. J. Crutzen, Sulfur dioxide in remote oceanic air: Cloud transport of reactive precursors, *J. Geophys. Res.*, *89*, 7111–7132, 1984.

Chatfield, R. B., and A. C. Delany, Convection links biomass burning to increased tropical ozone: However, models will tend to overpredict O_3, *J. Geophys. Res.*, *95*, 18,473–18,488, 1990.

Dickerson, R. R., et al., Thunderstorms: An important mechanism in the transport of air pollutants, *Science*, *235*, 460–465, 1987.

Fishman, J., C. E. Watson, J. C. Larsen, and J. A. Logan, Distribution of tropospheric ozone determined from satellite data, *J. Geophys. Res.*, *95*, 3599–3618, 1990.

Fishman, J., V. G. Brackett, E. V. Browell, and W. B. Grant, Tropospheric ozone derived from TOMS/SBUV measurements during TRACE A, *J. Geophys. Res.*, this issue.

Grell, G. A., J. Dudhia, and D. R. Stauffer, A description of the fifth-generation Penn State/NCAR mesoscale model (MM5), *NCAR Tech. Note, NCAR/TN-398+STR*, Natl. Cent. for Atmos. Res., Boulder, Colo., 1994.

Heikes, B. G., et al., Hydrogen peroxide and methylhydroperoxide distributions related to ozone and odd hydrogen over the North Pacific in the fall of 1991, *J. Geophys. Res.*, *101*, 1891–1905, 1996.

Jacob, D. J., et al., Origin of ozone and NO, in the tropical troposphere: A photochemical analysis of aircraft observations over the South Atlantic basin, *J. Geophys. Res.*, this issue.

Justice, C. O., J. D. Kendall, P. R. Dowty, and R. J. Scholes, Satellite remote sensing of fires during the SAFARI campaign using NOAA AVHRR data, *J. Geophys. Res.*, this issue.

Kirchhoff, V. W. J. H., and E. V. A. Marinho, Layer enhancements of tropospheric ozone in regions of biomass burning, *Atmos. Environ.*, *28*, 69–74, 1994.

Kirchhoff, V. W. J. H., J. R. Alves, F. R. de Silva, J. Fishman, Observations of ozone concentrations in the Brazilian cerrado during the TRACE A field expedition, *J. Geophys. Res.*, this issue.

Lacis, A. A., D. J. Wuebbles, and J. A. Logan, Radiative forcing of climate by changes in the vertical distribution of ozone, *J. Geophys. Res.*, *95*, 9971–9981, 1990.

Luke, W. T., R. R. Dickerson, W. F. Ryan, K. E. Pickering, and L. J. Nunnermacker, Tropospheric chemistry over the lower Great Plains of the United States, 2, Trace gas profiles and distributions, *J. Geophys. Res.*, *97*, 20,649–20,670, 1992.

O'Sullivan, D., M. Lee, K. B. Noone, and B. G. Heikes, Henry's Law solubilities for hydrogen peroxide, methylhydroperoxide, hydroxymethylhydroperoxide, ethylhydroperoxide, and peroxyacetic acid in water, in press, *Environ. Sci. Technol.*, 1995.

Pickering, K. E., A. M. Thompson, R. R. Dickerson, W. T. Luke, D. P. McNamara, J. Greenberg, and P. R. Zimmerman, Model calculations of tropospheric ozone production potential following observed convective events, *J. Geophys. Res.*, *95*, 14,049–14,062, 1990.

Pickering, K. E., A. M. Thompson, J. R. Scala, W.-K. Tao, J. Simpson, and M. Garstang, Photochemical ozone production in tropical squall line convection during NASA/GTE/ABLE 2A, *J. Geophys. Res.*, *96*, 3099–3114, 1991.

Pickering, K. E., A. M. Thompson, J. R. Scala, W.-K. Tao, and J. Simpson, Ozone production potential following convective redistribution of biomass burning emissions, *J. Atmos. Chem.*, *14*, 297–313, 1992a.

Pickering, K. E., J. R. Scala, A. M. Thompson, W.-K. Tao, and J. Simpson, A regional estimate of convective transport of CO from biomass burning, *Geophys. Res. Lett.*, *19*, 289–292, 1992b.

Pickering, K. E., A. M. Thompson, D. P. McNamara, M. R. Schoeberl, H. E. Fuelberg, R. O. Loring Jr., M. V. Watson, K. Fakhruzzaman, and A. S. Bachmeier, TRACE A trajectory intercomparison, 1, Effects of different input analyses, *J. Geophys. Res.*, this issue.

Prins, E. M., and W. P. Menzel, Trends in South American biomass burning detected with the GOES visible infrared spin scan radiometer atmospheric sounder from 1983 to 1991, *J. Geophys. Res.*, *99*, 16,719–16,735 1994.

Tao, W.-K., and J. Simpson, The Goddard cumulus ensemble model, 1, Model description, *Terr. Atmos. Oceanic Sci.*, *4*, 35–72, 1993.

Smyth, S., et al., Factors influencing the upper free tropospheric distribution of reactive nitrogen over the South Atlantic during the TRACE A experiment, *J. Geophys. Res.*, this issue.

Thompson, A. M., K. E. Pickering, D. P. McNamara, M. R. Schoeberl, R. D. Hudson, J. H. Kim, E. V. Browell, V. W. J. H. Kirchhoff, and D. Nganga, Where did tropospheric ozone over southern Africa and the tropical South Atlantic come from in October 1992? Insights

from TOMS, GTE/TRACE A and SAFARI 1992, *J. Geophys. Res.*, this issue.

Wang, Y., W.-K. Tao, K. E. Pickering, A. M. Thompson, J. S. Kain, R. F. Adler, J. Simpson, P. R. Keehn, and G. S. Lai, Mesoscale model (MM5) simulations of TRACE A and PRESTORM convective systems and associated tracer transport, *J. Geophys. Res.*, this issue.

Watson, C. E., J. Fishman, and H. G. Reichle Jr., The significance of biomass burning as a source of carbon monoxide and ozone in the southern hemisphere tropics: A satellite analysis, *J. Geophys. Res.*, 95, 16,443–16,450, 1990.

D. R. Blake, University of California-Irvine, Irvine, CA 92717.

J. D. Bradshaw, Georgia Institute of Technology, Atlanta, GA 30332.

G. L. Gregory and G. W. Sachse, NASA Langley Research Center, Hampton, VA 23681.

B. G. Heikes, Graduate School of Oceanography, University of Rhode Island, Narragansett, RI 02882-1197.

V. W. J. H. Kirchhoff, INPE, Sao Jose dos Campos, SP, Brazil.

D. P. McNamara, Applied Research Corporation, Landover, MD 20785.

K. E. Pickering (corresponding author), Joint Center for Earth System Science, Department of Meteorology, University of Maryland, Code 916, College Park, MD 20742.

W. K. Tao and A. M. Thompson, NASA Goddard Space Flight Center, Greenbelt, MD 20771.

Y. Wang, Science, Systems, and Applications, Inc, Lanham, MD 20706.

(Received April 12, 1995; revised December 29, 1995; accepted December 29, 1995.)